STUDY AND INVESTIGATIONS OF DUAL BAND MICROSTRIP PATCH ANTENNAS LOADED WITH SPLIT RING RESONATORS

A THESIS SUBMITTED IN PARTIAL FULFILMENT DF THE REQUIREMENTS FDR THE AWARD DF DEGREE DF

Master of Engineering

IN

WIRELESS COMMUNICATION

by

Deepak

Roll No. 801363008

Under the guidance of

Dr. Jaswinder Kaur

Lecturer, ECED

Thapar University, Patiala

ELECTRONICS AND COMMUNICATION ENGINEERING DEPARTMENT

THAPAR UNIVERSITY

(Established under the section 3 of UGC Act, 1956)

PATIALA – 147004, PUNJAB, INDIA

JULY 2015

Declaration

I, Deepak, hereby declare that this thesis, which is being presented, entitled **"Study and Investigation of Dual Band Microstrip Patch Antennas Loaded with Split Ring Resonator"** by me for the consideration of the requirements for the award of degree in Master of Engineering in Wireless Communication from Thapar University, Patiala, is an original record of my own work, under the supervision of **Dr. Jaswinder Kaur**, Lecturer, Electronics and Communication Engineering Department.

The matter presented has not been submitted in any other University/ Institute for the award of any other degree.

Date: 15/7/'15

Deepak

Roll no: 801363008

This is to certify that the above statement made by this student is correct to the best of my knowledge and belief.

Date: 15/7/'15

Dr. Jaswinder Kaur

Lecturer

ECED

Thapar University, Patiala

Countersigned by:

(Dr. Sanjay Sharma)

Professor and Head, ECED

Thapar University, Patiala

(Dr. S. S. Bhatia)

Dean of Academic Affairs

Thapar University, Patiala

Acknowledgements

I pay my sincere thanks to the supervision of the faculty of my department, support from my family, and help from friends, without whom this thesis would not be completed.

I utter my deepest thankfulness to my guide, **Dr. Jaswinder Kaur**, Lecturer, ECED, Thapar University, Patiala, for her splendid guidance, patience, caring, and providing me an excellent atmosphere for the research work.

I thank **Dr. Sanjay Sharma**, Professor and Head, ECED, Thapar University, Patiala, for granting us with sufficient facilities and infrastructure to carry our work.

I would like to acknowledge **Dr. Hemdutt Joshi**, Assistant Professor and Program Coordinator (WC), ECED, Thapar University, Patiala, for being a source of inspiration for us during our research work.

I sincerely thank **Dr. Rajesh Khanna**, Professor, ECED, Thapar University, Patiala, for the support he has bestowed, as well as, for the establishment of antenna research lab and an environment of antenna research in Thapar University, Patiala.

Abstract

This work has been focused mainly upon analyzing a rectangular microstrip patch antenna loaded with various combinations and configurations of a complementary split ring resonator, or a meander line, or a stepped-impedance filter. Cavity model has been used for visualization purposes, whereas Finite Difference Time Domain method has been used through software CST Microwave Studio® for calculation/simulation purposes. ISM bands of frequencies have been used, as they require no licensing permissions. New designs have been simulated, fabricated, and tested for the validation of their results.

Contents

List of Tables

List of Figures

Keywords

Complementary Split Ring Resonators, Meander Line antenna, Microstrip Patch antenna, Stepped Impedance Low Pass filter, Slotted antenna, WLAN.

Notation and Abbreviations

α	Alpha
δ	Delta
ϵ_r	Relative Dielectric Constant
α_t	Thermal Expansion Coefficient
f_0	Resonant Frequency
ABC	Absorbing Boundary Condition
CSRR	Complementary Split Ring Resonator
CST®	Computer Simulation Technology
dB	deci-Bel
DGS	Defected Ground Structure
EBS	Electronic Band Structure
EM	Electro Magnetic
EM	Electro-Magnetic
EMW	Electro Magnetic Wave
etc.	Etcetra

FDTD	Finite Difference Time Domain
FR-4	Flame Retardant 4
GSM	Global System for Mobile Communications
HAC	Hearing Aid Compatibility
Lab.	Laboratory
LPF	Low Pass Filter
MLA	Meander Line Antennas
MOM	Method of Moments
MPA	Microstrip Patch Antenna
MSA	Microstrip Antenna
NITTTR	National Institute of Technical Teachers Training & Research
NMSU	New Mexico State University
PIFA	Planar Inverted F Antenna
PTFE	Polytetraflouroethylene
RFID	Radio Frequency Identification
RIS	Reactive Impedance Surface
SAR	Specific Absorption Rate
SRR	Split Ring Resonator
TLM	Transmission Line Model
UMTS	Universal Mobile Telecommunications System

UWB	Ultra Wide Band
VNA	Vector Network Analyzer
WLAN	Wireless Local Area Network

Chapter 1

Introduction

1.1 History of MPAs

The concept of Microstrip antenna was first introduced in around 1953, when Deschamps [1] from U.S.A. , & Gutton and Baissionot [2] from France presented their work. Then agin in 1970's, the work on Microstrip Antennas was kick-started when Byron [3] presented a Strip Radiator(conducting) and Ground separated by dielectric substrate. This periodic array was used for Project Camel, where coaxial feed was given at periodic intervals. Shortly after that, Munson [4] patented a Microstrip element. Thereafter, MPA was used in Rockets(array design), K-135 aircraft(conformal array), ATS Satellite, Missiles etc. giving rise to a new Industry, The Antenna Industry.

Lo *et al.* [5] published the first mathematical analysis using model-expansion techniques to analyze a large variety of MPAs- Square, Rectangle,Circle,Semicircle,triangle patch shapes. New Mexico State University , Las Cruces; co-sponsorship U.S. Army Research Office and Physical Science Lab. NMSU, witnessed the first International meeting on Microstrip Antenna designs, materials,theoretical models, and array configurations.

1.2 Effects of substrate's material

Dependence of operating frequency on the thin substrate's dielectric constant [6] [7] [8] is as follows:

$$\frac{\delta f}{f_0} = -\frac{1}{2}\frac{\delta \epsilon_r}{\epsilon_r} \tag{1.1}$$

where, δ denotes the changes in parameter, present in it's argument, f denotes the operating frequency, f_0 denotes the resonant frequency, ϵ_r denotes the relative dielectric constant of the substrate. This equation **??** includes only small tolerable changes, which shows that operating frequency is highly sensitive to changes in dielectric constant of substrate material.

Dependence of operating frequency on substrate's thickness(here denoted by l), or it's temperature is as follows:

$$\frac{\delta f}{f_0} = -\frac{\delta l}{l} = -\alpha_t \delta T \tag{1.2}$$

where T is the temperature of substrate in degree Celsius & α_t is the thermal expansion coefficient of substrate.

Generally regarding the substrate material, we talk about it's dielectric constant and loss tangent [9] [10] [11] [12] . Substrates are usually Polytetraflouroethylene (PTFE) with reinforced material as woven glass, or woven fiber, or ceramic etc. These filler materials follow a preferred orientation while manufactured, because we have dielectric constant dependence on orientation of electric field with higher value observed electric field along sheet's plane instead of transverse to sheet. Usually the manufacturers quote the dielectric constant for electric field perpendicular to sheet, measured using stripline resonator technique [13]. Dielectic constant of PTFE substrate based materials have a tendency to decrease with increase in temperature.

Combining 1.1 & 1.2 we obtain

$$\frac{\delta f}{f_0} = \left(-\alpha_r + \frac{1}{2}\alpha_E\right)\delta T \tag{1.3}$$

1.3 Advantages/Disadvantages of MPA

1.3.1 Advantages of MPA

Various advantages of MPAs are:

1. They are planar and can easily be made conformal to a surface, which is highly required for aerodynamic applications.
2. They have a low profile.
3. They are rugged and strong.
4. They exhibit a lower radar cross section, good for some defense applications.
5. They can be manufactured using printed circuit technology, that easy to integrate with present electronic systems.
6. Can be easily designed for multiple frequency applications.
7. Dual polarization can be easily achieved.

1.3.2 Disadvantages of MPA

MPAs have some disadvantages also. Some of them are:

1. In the basic form of MPA, it has a narrow impedance bandwidth, usually less than 5%. Although, we have techniques to improve this, but sacrifices is in the form of increased antenna volume.
2. Usually, it can handle powers in the order of tens of watts. This low power handling capacity is due to very less distance between the radiating patch and the ground below.
3. As compared to the array network of other type of antennas, MPA arrays show higher ohmic losses, due to losses in dielectic substrate, feed conductors, and power dividing circuits.

Table 1.1: Band Designations

Band Designations	
Name of the Band	Frequency Range (in GHz)
Band-L	1-2
Band-S	2-4
Band-C	4-8
Band-X	8-12
Band-K_u	12-18
Band-K	18-26
Band-K_a	26-40
Band-U	40-60

4. In basic form, it posses lower efficiency.

5. Although polarization is easily achieved, its purity is poorer than the other methods followed commercially.

1.4 Frequency band allocations

Frequency spectrum is a very important natural resource. Every instrument has a specific and fixed frequency band, over which it works. Frequency allocation done for commercial purpose usually involves very high cost. Frequency allocation/distribution is decided globally in a unison, and government of each country further allocates it for its development purposes. Various names are assigned to various bands [14] shown in Table 1.1, frequency allocation for licensed [15] and unlicensed [15] bands are shown in Table 1.2 and Table 1.3 respectively. Now a days, a large number of softwares [14] are available for EM simulations, a list is given in Table 1.4.

CST Microwave Studio® 2014 [16] has been used for all simulation work in this thesis. Introducing the moment, before Method of Moments are considered in detail in method of analysis chapter.

Table 1.2: Licensed Spectrum

U.S. Licensed spectrum allocations	
Service/system	**Frequency span**
AM radio	535-1605 kHz
FM radio	88-108 MHz
Broadcast TV channels 2-6	54-88 MHz
Broadcast TV channels 7-13	174-216 MHz
Broadcast TV UHF	470-806 MHz
Broadband wireless	746-764 MHz, 776-794 MHz
Broadband wireless-3G	1.7-1.85 MHz, 2.5-2.69 MHz
Digital cellular phones-1G and 2G	806-902 MHz
Personal communication systems 2G cell phones	1.85-1.99 GHz
Wireless communications service	2.305-2.32 GHz, 2.345-2.36 GHz
Satellite digital radio	2.32-2.325 MHz
Multichannel multipoint distribution service-MMDS	2.15-2.68 MHz
Digital broadcast satellite TV	12.2-12.7 GHz
Local multipoint distribution service-LMDS	27.5-29.5 GHz, 31-31.5 GHz
Fixed wireless services	38.6-40 GHz

1.4.1 Moments

Moments[17] are used many a times, when we are dealing with non-deterministic signal analysis. By definition moment is

$$m_n = E\{\mathbf{x}^n\} \tag{1.4}$$

$$= \int_{-\infty}^{\infty} x^n f(x)\mathrm{d}x \tag{1.5}$$

whereas the Central moment is defined as

$$\mu_n = E\{(\mathbf{x}-\eta)^n\} \tag{1.6}$$

$$= \int_{-\infty}^{\infty} (x-\eta)^n f(x)\mathrm{d}x \tag{1.7}$$

Table 1.3: Unlicensed Spectrum

U.S. Unlicensed spectrum allocations	
Band	**Frequency span**
ISM band 1-cordless phones, 1G WLANs	902-928 MHz
ISM band 2-Bluetooth, 802.11b and802.11a WLANs	2.4-2.4835 GHz
ISM band 3-wireless PBX	5.725-5.85 GHz
U-NII band 1 indoor systems, 802.11a WLANs)	5.15-5.25 GHz
U-NII band 2 short-range outdoor systems, 802.11a WLANs)	5.25-5.35 GHz
U-NII band 3 long-range outdoor systems, 802.11a WLANs)	5.725-5.825 GHz

In a similar fashion Absolute moment is defined as $E\{|x|^n\}$ or $E\{|x-\eta|^n\}$,
and Generalized moment as $E\{(x-a)^n\}$ or $E\{|x-a|^n\}$,
where $\mathbf{x}$ is a random variable with probability density function $f(x)$, whereas the expectation or mean function is denoted by $E\{x\}$ or η which is defined as

$$E\{\mathbf{x}\} = \int_{-\infty}^{\infty} x f(x) \mathrm{d}x \tag{1.8}$$

1.5 Split Ring Resonators

SRRs [18] is a type of metamaterial [19], which is an artificial structure possessing EM properties, not usually found in nature. SRRs are specifically shows double negativity, in the sense that it's permittivity as well as permeability are both negative, at frequencies of concern. The effect of this simultaneous negative permittivity, permeability is that, it produces a backward wave propagation. Direction of propagation of backward wave propagation is not decided by right hand rule but by left hand rule, that is the wave vector's direction is obtain by using left hand rule for cross product of electric field with magnetic field. In other sense, the product of group velocity and phase velocity is negative. This is also the reason, why SRRs are also called Left handed materials. The effect of these SRRs can easily be observed as inversion in Snell's law, backward Cherenkov radiations, inversion in Doppler effect. Advantage of SRRs over other metamaterials is

Table 1.4: Commercial EM softwares

Software Name	**Theoretical Model**	**Company**
Microwave Studio	FDTD	CST
IE3D	Moment method	Zealand
Ensemble	Moment method	Ansoft
EM	Momentum method	Sonnet
Momentum	Moment method	HP
FEKO	Moment method	EMSS
PiCasso	Genetic/Moment method	EMAG
Micropatch	Segmentation	Microstrip design, Inc.
PCADD	Cavity model	Antenna design associates
HFSS	Finite element	Ansoft
Fidelity	FDTD	Zealand

that they can be easily fabricated on planar structures, without disturbing its profile. Equivalent circuit [18] of SRRs is a L-C resonator circuit, which can be excited by an external magnetic field, as well as by a time varying properly polarized electric field. CSRRs are complementary to the SRR in the sense that the metal shape of SRR in the patch replaced by a similar shaped slot in the ground below it, produces similar resonating frequencies.

Chapter 2

Literature Survey

Paper by Carver *et al.* [20] is the most cited paper in MSA. They have surveyed some designs & some arrays, based on various parameter variations. They also surveyed various methods of analysis, including both theoretical as well as practical methods.Various applications & scope in future applications have also been discussed here.This paper serves as a basic paper to understand higher complexity in MSA.

In [21], a magnetic superstrate material has been engineered to improve efficiency and gain of MPA , without any significant change in the profile or size of the antenna. Along with magnetic superstrate inclusions of modified Split Ring Resonators is also done. Numerical method of analyses is used to analyze the whole structure. The proposed antenna operates in UMTS band, 3.4 dB of antenna gain improvement in broadside has been observed along with 17 % improvement in the efficiency, where the total height used is only $\lambda_0/7$, λ_0 being the wavelength in free-space at resonance frequency.

In [22], the analyses of mutual coupling between microstrip patch antennas is done. The authors have shown a decrease in the mutual coupling with increase in distance, in a monotonic behavior. It has been shown that for 1/16 inches and 1/8 inches substrates, space wave coupling mechanism dominates surface wave coupling in L-band because surface wave are negligible for these cases. 1.40 to 1.45 Ghz range of frequency is used for calculation of S parameters for an array of two elements. This array can be square array, rectangular array, or circular array which are oriented for adjacent H-plane or E-plane

edges. A large aluminum plane placed rigidly is used as a ground plane. Complex S parameter calculation is for the variation in spacing, that is a function with respect to spacing is formulated. To provide continuation of substrate, insertion of dielectric spacers is done, with the data being observed using Vector network analyzer. The authors have first taken the general case of mutual coupling due to both surface wave and space wave, and their sensitivities are calculated. A five element Dolph Tchebyscheff linear array is also used to investigate effect of mutual coupling.

In [23], a broadband antenna configuration is presented to decrease the mutual coupling between antenna elements. Since the structure is broadband, it can be used for multiband mutual coupling reduction. Two CSRRs are loaded on two antennas, connected further with an additional slot, to decrease the coupling. 10 dB reduction for the patches with 1/4 times freespace wavelength apart have been achieved. When the antennas are placed in near field zone, their near field coupling is considered, which are more pronounced when the permittivity of substrate is very low. Whereas space wave shows dominance in the case of close proximity. Eigenmode analysis using CST Studio has been demonstrated. Due to the loading of slotted CSRRs, slight change in the resonant frequency is also observed. CSRRs connected through slots are viewed as cascaded filters, another reason for using slot in the ground plane is dictated as to provide a low pass filter response for some frequencies of interest.

In [24], response of designing geometrical shapes on a defected ground structure is observed, mainly on a microstrip Hi-Lo Low pass filter. 67 % reduction in electrical length has been observed with DGS as compared to that without it, observed with a focus on three pole LPF. Rejection in the stop band of LPF has been observed, which also changes with the change in shape of the slot. Four different shapes, arrowhead slot, rectangular slot, square head slot, and dumb bell slot of DGS has have been employed, with the results mainly been observed with CST Studio. DGS slots have been modeled as LC resonance tank circuits.

In [25], the authors have designed, fabricated and tested six variations of a design of MPA, stacked in the layers as ground in the bottom covered by a dielectric substrate,

covered by a RIS slotted metal layer, again covered by the dielectric substrate, covered by the patch which is loaded with two CSRRs. The orientation of these CSRRs are changed in the ways, like changing the relative positions of the slots in outer and inner ring of CSRRs, also changing their absolute position. Changes in the location of feed has also been observed, the feed used is coaxial feed, as it gives better result as compared to strip line feed in the case concerned. CST Studio is used to observe the reflection coefficients and pattern of radiation. Since only one port is used, its mainly $|S_{11}|$ dB, which is observed. These CSRRs are observed to behave as LC tank resonator circuits, loading the MPA. RIS has further been used to improve the control over inductance of the design. RIS here mainly works as an EBG structure.

In [26], a dualband planar antenna array has been proposed for WLAN applications. Focus is given on the current distribution for various frequencies of interest. The structure is a modified step impedance structure. Dimensions of a step impedance filter are changed, it is then rotated to get improved results and then arranged as to make an array for getting good directional gain as well as good (less) return loss. Structure is fed with a coaxial cable. Structure being symmetric across y-axis, the current through the strip lines are managed, using their length, such that the lower part is 180° out of phase with the upper half array structure. Point to point communication through WiFi has been materialized here.

In [27], the authors have demonstrated a beautiful property of meander line- the polarization. Here various metallic meander lines, with proper spacing are placed on a sheet, and stacking of one sheet over the other is done upto some number of layers. When an Electromagnetic wave falls on this polarizer, wave components of one direction are advanced in phase, whereas the wave components in its perpendicular direction are delayed in phase. Thus a phase difference is created between two components in perpendicular direction. So, this polarizer made up of stacked layer of meanderlines keeps on purifying the incident wave into two polarized wave, polarized in two perpendicular directions. Analyses is done for the EM waves in X-band.

In [28], a design for RFID application is presented, where impedance matching between

the antenna and chip is focused upon. SRRs are used as resonating elements and loads the patch, making impedance matching easier. 815 MHz and 915 MHz frequencies are used for RFIDs. Since the RFID are usually manufactured in bulk, because of their high practical use modern identification system, providing a proper conjugate matching would improve it's efficiency. Circular SRRs are used to provide a positive phase to the network, providing smaller phase for the upper frequency.

In [29], an interdigital capacitance in the form of meander line slot is made on the top metal, whereas etching of CSRRs is done on the bottom plane. Hybridizations of TM_{01} and TM_{10} modes is done here to yield a wideband radiation pattern. 96 % has been observed with a gain of 3.85 dBi with a very small sized antenna. Here, interdigital structure provides series capacitance, and CSRRs are used to provide shunt admittance, giving series LC circuit and shunt LC resonator in the equivalent model of the designed MPA. CST studio has been used for getting the expected result.

In [30], a design for beam steering is presented. Beam steering is widely used in defense sector in radars, where a radar needs to steer its beam for surveillance purposes. In past mechanical steering was used, but with the advancement of technology steering of beam is done electronically using phased array radars. In this design, CSRR is loaded on ground to provide a wide steering angle with a reduced size, thus making some reduction in the cost of phased array systems. It is also shown that beam direction is affected by reflective index of loading section. A scan from $-50°$ to $48°$ is presented, with only change involved is CSRR parameters. No phase shifters are used. This structure is light, low profile and good for communication systems, where beam steering is required.

In [31], changes in the radiation parameters of an UWB antenna is studied with respect to changing substrate material. Variation in the substrate is done in it's thickness and its material. Circular monopole configuration is used for the antenna. Loss tangents are given proper concern, and simulation results are obtained through IE3D software. Various forms of FR-4, foam, and duroid materials are used for understanding the variations due to substrate material.

In [32], wide area network of mobile wireless technology is achieved using a small sized

PIFA operating at $\lambda/8$ mode as fundamental resonant mode. A coupling feed is used to fed two strips of $\lambda/8$ at frequency 900 MHz. This coupling feed has largely decreased input impedance as that compared with simple feed. Higher modes of $\lambda/4$ are also observed, forming band for GSM operations. SAR values and HAC values are also calculated.

Chapter 3

Methods of Analysis

3.1 Transmission-Line Model

3.1.1 Model and various Parameters

This model utilizes Transmission line Theory. Of the total four edges of Rectangular Microstrip Patch Antenna, only two of them effectively radiates; these two parallel edges are modeled as two parallel radiating slots [33]. These radiating slots, each of length a radiates in upper half plane, restricted by ground in the lower half, with admittance as [34]:

$$G_1 + jB_1 \cong \frac{\pi a}{\lambda_0 z_0}[\,1 + j(\,1 - 0.636 \ln k_0 w)\,] \tag{3.1}$$

where $z_0 = \sqrt{\frac{\mu_0}{\epsilon_0}}$, $k_0 = \frac{2\pi}{\lambda_0}$, slot width w, which is approximately equal to substrate thickness. Second slot is identical to first, if we neglect influence of feed on fringing field that side, So, similar equation holds for second slot.

Characteristic admittance is given as:

$$Y_0 = \frac{a\sqrt{\epsilon_r}}{t z_0} \tag{3.2}$$

where we have assumed that the field does not vary along the direction of radiating slot. It is desirous to excite both the slots 180° out of phase, for which the dimension b of

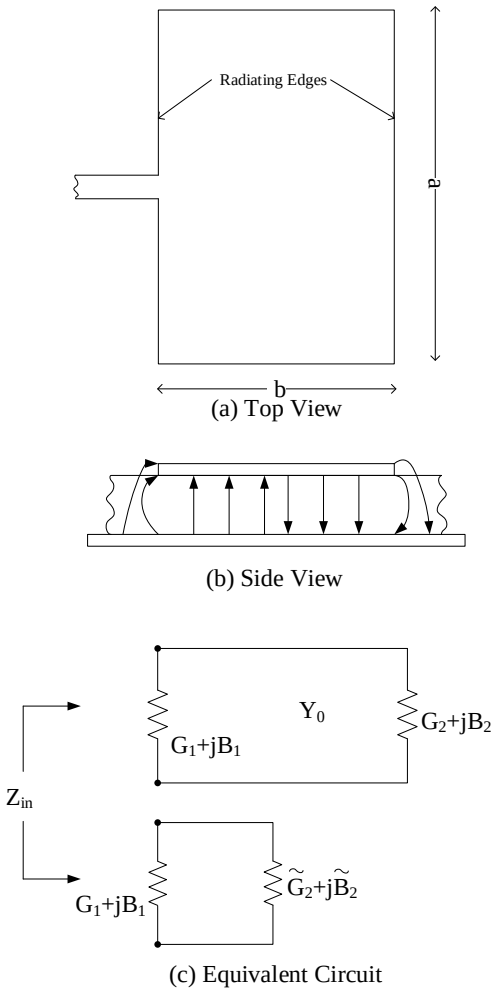

Figure 3.1: Transmission Line Model

patch should be a little less than $\frac{\lambda_d}{2}$, where $\lambda_d = \frac{\lambda_0}{\sqrt{\epsilon_r}}$ i.e $b = 0.48\lambda_d$ to $b = 0.49\lambda_d$. This little reduction is due the effect of fringing fields. By properly selecting these parameters, we get the admittance [35] of second slot as:

$$\widetilde{G_2} + j\widetilde{B_2} = G_1 - jB_1 \tag{3.3}$$

Therefore the total input admittance, at resonance is as

$$Y_{in} = (\, G_1 + jB_1) \, + (\, G_2 + jB_2) \, = 2G_1 \tag{3.4}$$

If we consider $a = \frac{\lambda_0}{2}$, then G_1 becomes 0.00417 mhos, and

$$R_{in} = \left(\frac{1}{2G_1}\right) = 120\ \Omega \tag{3.5}$$

For resonant frequency we know that

$$f_r = \frac{c}{\lambda_d\sqrt{\epsilon_r}} = q\frac{c}{2b\sqrt{\epsilon_r}} \tag{3.6}$$

3.5 and 3.6 gives us a simple formula to calculate input resistance and resonant frequency, q in 3.6 refers to the fringing factor arising due to the fringing effect involved. This q is first calculated experimentally, then same q is taken for the patch of other dimensions but same substrate and in above same frequency range.

Transmission Line Model proposed by Munson [33] had three drawbacks:

1. For narrow patches(width$\leq \lambda_0$), expression for radiation admittance Y_t are inaccurate.

2. Mutual coupling radiating slots was neglected.

3. Effects of side slots on radiation conductance are neglected.

Pues *et al.* rectified above mentioned problem to a good level. As shown in Figure 3.2, where Y_s is self-admittance of main radiating slots, Y_m is mutual radiative admittance between them, and mutual coupling is taken into account using Voltage-Controlled-Current Source.

Line parameters can be written, using planar waveguide model [36] as:

$$Z_c = \frac{\eta_0}{\sqrt{\epsilon_{re}}}\frac{h}{W_e} \tag{3.7}$$

$$\beta = k_0\sqrt{\epsilon_{re}} \tag{3.8}$$

$$\alpha = 0.5\beta\tan\delta_e \tag{3.9}$$

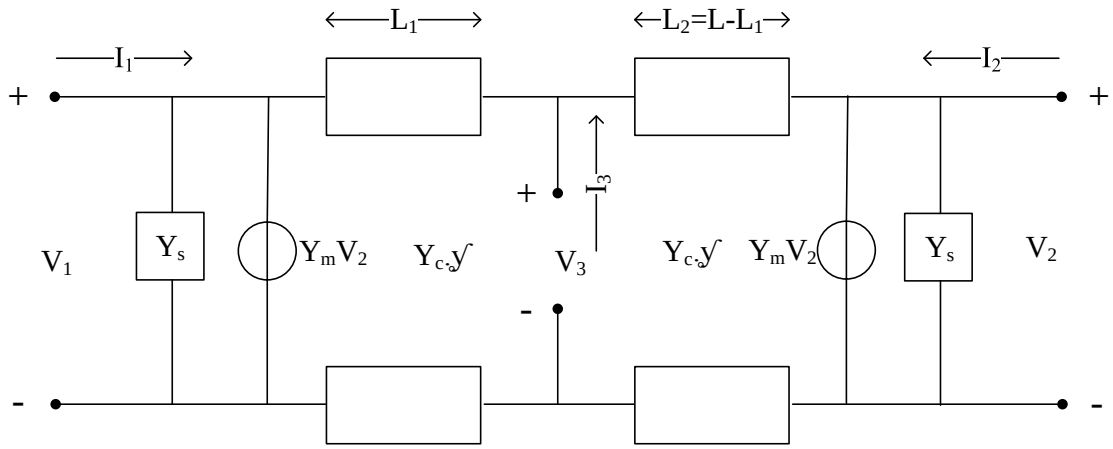

Figure 3.2: Improved Transmission Line Model as three port

where,

$\eta_0 = \sqrt{\frac{\mu_0}{\epsilon_0}}$= free space wave impedance.

$k_0 = \frac{2\pi}{\lambda_0}$= wave number in free space.

W_e = effective width. ϵ_{re}= effectove dielectric constant.

$\tan\delta_e$= effective loss tangent.

Their accurate formulas can found in literature [37].

For determining Self admittance $Y_s = G_s + jB_s$, Deneryd [38] model has been modified. For self susceptance B_s, the transmission-line formula is:

$$B_s = Y_s \tan(\beta \Delta l) \tag{3.10}$$

where, Δl is open end extension of patch considering semi-infinite microstrip line of width W.

3.1.2 Drawbacks

The drawback of this Transmission Line Model is that, it can not properly predict the input characteristics of an antenna for frequency, which are far away from the fundamental resonant frequency, making this model not suitable for predictions in case of higher mode [39] frequencies. Also, it works good mainly when we have emperically found the fringe factor, that is it ignores radiating edge field variation, also, this model does not properly accomodate for the changes i n feed employed. To sort out these problems, we can move to another model for microstrip patch antenna.

3.2 Cavity Model

3.2.1 The Model

Lo, Solomon and Richards [40] proposed this model based on the following observations:

1. Since, the distance between patch on the top, and ground on the bottom is very small, Electric field has only z component and Magnetic field is aligned in x-y plane, within this cavity.

2. At all the frequencies of interest, Electro-Magnetic(EM) field is independent of the z co-ordinate within this cavity formed between the ground and the patch.

3. In microstrip, any point on edge must not have any electric current component perpendicular to the edge, that is tangential component of Magnetic field along the edge should be negligible or zero.

As mentioned, Figure 3.3 shows the MPA surrounded above by a metallic patch, below by a metallic ground, and the space between these is loaded by a dielectric material. A perfect conducting metal reflects [41] all the wave incident on it (with a skin depth of zero), that is magnitude of reflected electric field is same as that for incident electric field. So, according to this cavity model, the cavity is bounded by above by Electric plane, below by Electric plane, and by magnetic planes from the sides. This model has

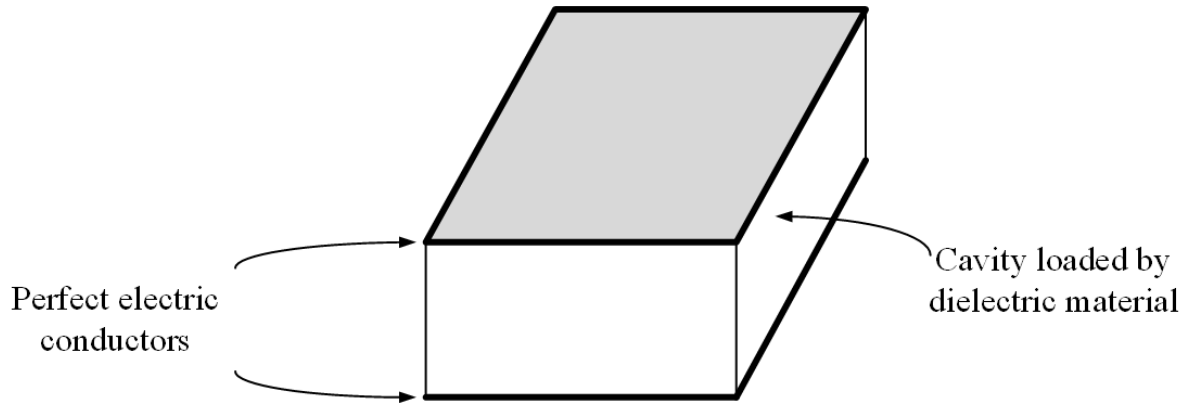

Figure 3.3: Cavity Model of a rectangular MPA

also been used to find lossy power reflective planes [42]. A slightly larger ground plane is considered to accommodate for the fringing fields. Various resonant modes[43] can exist within this cavity, for different dimensions of the MPA. With this model, the EM field distribution within this cavity is considered same as that on the patch, which is used to further calculate the various parameters required.

For this model,

$$\mathbf{E_m} = \psi_m \hat{\mathbf{z}} \tag{3.11}$$

$$\mathbf{H_m} = \hat{\mathbf{z}} \times \nabla_t \psi_m / j\omega\mu \tag{3.12}$$

$$\begin{aligned} (\nabla_t{}^2 + k_m{}^2)\psi_m &= 0, \quad \text{with } \frac{\partial \psi_m}{\partial n} && (3.13) \\ &= 0 \quad \text{on magnetic wall} && (3.14) \end{aligned}$$

where, $\mathbf{E_m}$, $\mathbf{H_m}$ are the electric field, magnetic field phasors, and ω is the angular frequency, and ∇_t is transverse part of del operator with respect to z-axis. The resonant wave number is

$$k_m = \omega_m \sqrt{\mu \epsilon_d} \tag{3.15}$$

where ϵ_d is the permittivity of the substrate. From Figure 3.4

$$\psi_{mn} = \cos \frac{m\pi}{a} x \, \cos \frac{n\pi}{b} y \tag{3.16}$$

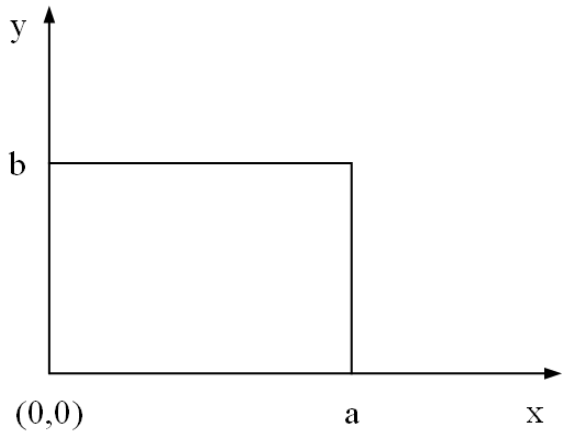

Figure 3.4: Dimensions used for calculating wavenumber

, and

$$k_{mn} = \sqrt{\left(\frac{m\pi}{a}x\right)^2\left(\frac{n\pi}{b}y\right)^2} \tag{3.17}$$

Wave equation of E_z in cavity for excitation current as $\mathbf{J}$ in $\hat{z}$ direction is given by

$$(\nabla^2 + k^2)E_z = j\omega\mu\mathbf{J}\cdot\hat{\mathbf{z}} \tag{3.18}$$

Application of this model is shown on a rectangular MPA with strip-line feed, shown in Figure 3.5. Here the feed dictates that

$$H_x = -1,\ c < x < d \text{ and } y = 0 \tag{3.19}$$

$$= 0\ ,\ x < c \text{ or } x < d, \text{ and } y = 0 \tag{3.20}$$

Y. T. Lo *et. al.* mentioned that

$$E_z = j\omega\mu\left\{\frac{d-c}{k^2ab} + \sum_{n=1}^{\infty}\frac{2(d-c)}{ab(k^2-{k_{0n}}^2)}\cos\frac{n\pi}{b}y + \sum_{m=1}^{\infty}\frac{4R_m}{m\pi b(k^2-{k_{m0}}^2)}\cos\frac{m\pi}{a}x + \sum_{m=1}^{\infty}\frac{8R_m}{m\pi b(k^2-{k_{m0}}^2)}\cos\frac{m\pi}{a}x\cos\frac{n\pi}{b}y\right\} \tag{3.21}$$

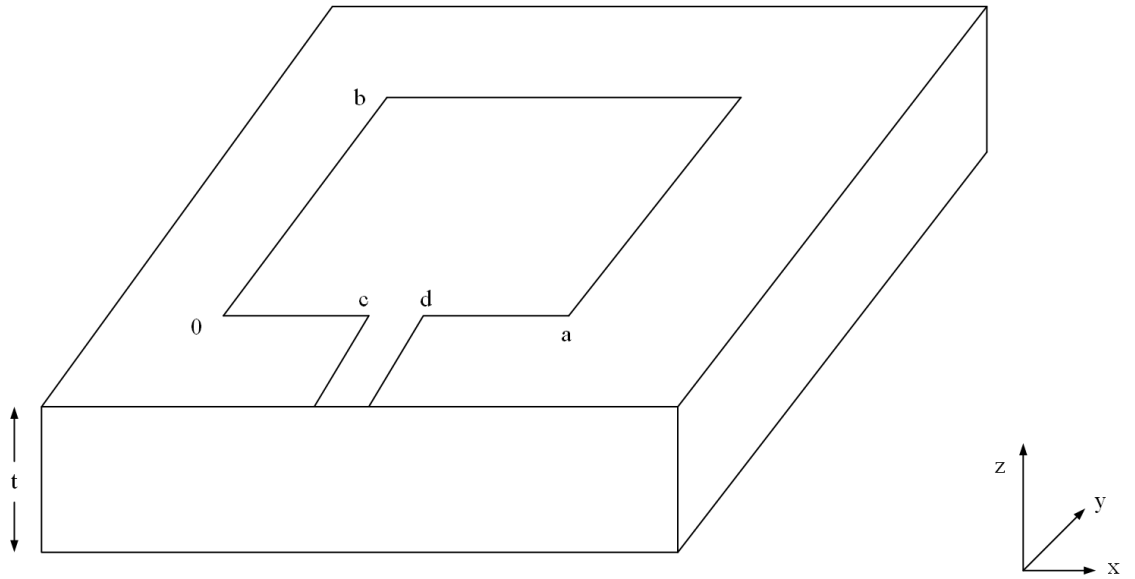

Figure 3.5: Rectangular MPA geometry

where

$$R_m = \sin\frac{m\pi}{2a}(d-c)\cos\frac{m\pi}{2a}(d-c) \tag{3.22}$$

$$k_{mn}{}^2 = \left(\frac{m\pi}{a}\right)^2 + \left(\frac{n\pi}{b}\right)^2 \tag{3.23}$$

The same formula can be worked out in a different manner, to follow the boundary conditions at magnetic walls $x = 0$, $x = a$, $y = 0$, $y = b$, the field in the cavity should have the form:

$$E_z = \sum A_m \cos\frac{m\pi}{a}x\cos\beta_m(y-b) \tag{3.24}$$

$$H_x = \frac{1}{j\omega\mu}\sum A_m\beta_m\cos\frac{m\pi}{a}x\sin\beta_m(y-b) \tag{3.25}$$

$$H_x = \frac{-1}{j\omega\mu}\sum A_m\frac{m\pi}{a}\sin\frac{m\pi}{a}x\cos\beta_m(y-b) \tag{3.26}$$

where,

$$\beta_m = \sqrt{k^2 - \left(\frac{m\pi}{a}\right)^2} \tag{3.27}$$

$$k = \omega\sqrt{\mu\epsilon_d} \tag{3.28}$$

$$A_0 = \frac{j(d-c)}{a}\sqrt{\frac{\mu}{\epsilon_d}\frac{1}{\sin kb}} \tag{3.29}$$

$$A_m = \frac{j4\omega\mu}{m\pi}\frac{\sin\frac{m\pi}{2a}(d-c)\cos\frac{m\pi}{2a}(d+c)}{\beta_m \sin\beta_m b} \tag{3.30}$$

where, $m = 1, 2, 3, ...$ Comparing equation 3.21 and 3.24, equation 3.21 gives a better insight but 3.24 converges faster, although both of them convey the same information.

3.2.2 Various Parameters

Since, in cavity model, the distance between the patch above and the ground below is very less, field is considered not to vary along the z-axis. Based on this logic, the field distribution on the patch is assumed to be same as that inside the cavity. Huygen's principle can be used to further calculate various radiation parameters. Electric vector potential, of huygen magnetic current source is

$$\mathbf{F(r)} = \epsilon_0 \int_C \frac{\mathbf{K(r1)}}{4\pi|\mathbf{r\text{-}r1}|} e^{-jk_0|\mathbf{r\text{-}r1}|} \mathrm{d}l(\mathbf{r1}) \tag{3.31}$$

where $\mathbf{K}$ is the magnetic current source. The far field at $\mathbf{r}$ is

$$E_\theta = \eta H_\phi = jk_0 F_\phi = jk_0(-F_x \sin\phi + F_y \cos\phi) \tag{3.32}$$

$$E_\phi = -\eta H_\theta = -jk_0 F_\theta = -jk_0(F_x \cos\theta\cos\phi + F_y \cos\theta \sin\phi) \tag{3.33}$$

The radiated total power is

$$P_r = \mathrm{Re}\int_0^{\pi/2}\int_0^{2\pi} (E_\theta {H_\phi}^* - E_\phi {H_\theta}^*) r^2 \sin\theta \,\mathrm{d}\phi\mathrm{d}\theta \tag{3.34}$$

In addition to this radiation, there are various losses involved like power loss due to energy dissipation in dielectric, electric conduction in wall and surface waves along substrate. so, the cavity model can be used to gain a better insight in the analysis of a microstrip patch antenna design, as the field distribution is same in the patch as well as inside the cavity. This surface wave loss is energy leaving cavity in form of guided waves along the

dielectric. Radiation loss is calculated from far zone EM field, whereas the dielectric loss and the conduction losses are calculated from the field inside the cavity.

3.2.3 Qualitative predictions

Following qualitative predictions can be made from the model described above, regarding a MPA:

1. A large number of resonant modes exist, each one characterized through a resonant frequency.

2. Since, fringing fields exist neat the edges, the MPA behaves as if its dimension is little larger. Semi-empirical formula can be used to make some modifications for effective dimensions.

3. Every mode has his own radiation pattern, the lower most one being strongest in radiation, with radiation in broadside direction with a beamwidth in 100° order.

4. For the coaxial fed MPAs, resonant modes depends on the location of feed point.

5. Bandwidth and quality factor are related to frequency, substrate permittivity and thickness through a complex function.

3.2.4 Limitations

Cavity model is based on the assumption that the thickness of substrate is very less, it has been observed that for the thickness of above 2% of free space wavelength, this model does not give good results. In many cases, the condition of magnetic wall gives some resonant frequencies, whose results does not match properly with that of practical results, in those cases some correction factor in various factors needs to be introduced. In case of stacked antennas, or in which we cover the patch with one more dielectric, this model doesn't work good because the height of cavity has been increased. Also, some problem has been found when using a coaxial feed, which is modeled as a thin current ribbon.

3.3 Semiempirical Models

Semiempirical models come midway between the empirical model and the full wave models, their computational complexity is more than that of empirical models but less than full wave models. Surface wave effect is taken into account into many of these models.

Variational Approach, this approach, suggested by Uzunoglu *et. al.* [41] was mainly for dipole elements, but it can be extended easily to other patch antennas. In this approach we first derive Green's function for horizontal Hertzian dipole, which is printed on ground substrate. We then write expression for antenna's input impedance using the assumed dipole current distribution along with the Green's function. In this model, usually based on quasi-TEM mode in microstrip, sinusoidal current distribution is assumed on the dipole. It involves numerical computation of improper integrals in two dimension. Input impedance's real part is the superposition of space wave and surface wave components, this way explicit equations are derived for far field components of radiation field.

Generalized Variational Approach, this method was suggested by Suzuki *et. al.* [44] which uses modal expansion technique in addition to the above mentioned method. Here again the assumptions of thin substrate material and magnetic walls are made, where it finally gives us a network model with various ports for the microstrip patch antenna given. It shows good handling of multiport networks connectivity. Various steps involved in this method are:

1. With electical thin substrate assumption, quasi-TEM mode propagation is taken, that is only H_x, H_y and E_z are considered non-zero.

2. Scalar Helmholtz equation's solution is considered for perfect magnetic wall condition. This gives E_z as double integral over patch surface, which is product of Green's function and the function representing distribution of surface wave current on the patch.

3. Rayleigh-Ritz method and standard form of variational formulation are used to calculate eigenmodes and eigenvalues involved in Green's function.

4. Since, the Green's function is known now, so we can easily calculate other field components.

But since this method also uses assumption of electrical thin substrate and perfect magnetic wall, its applicability above 30 GHz is not reliable.

3.3.1 Approach of Dual Integral Equation

Proposed by Chew *et. al.* [45], they mainly analyzed a vertical prob fed circular patch antenna. Current on the probe is assumed uniform and the metalization thickness is assumed to be 0. Analysis is done as:

1. First, consider only the probe present inside the dielectric with ground at the base, but no patch over it. Then, z-component of Electric field is calculated using formulation of dyadic Green's function in Hankel vector transform domain.

2. Next, we introduce the patch, computing the induced current over it, assuming that the probed is located symmetrically, the field due to these induced current are then derived.

3. Standard Galerkin's method is then used along with the assumptions of suitable boundary conditions, getting euqtions in vector dual integral, which are solved to get patch current.

4. Since, we got the patch current, radiation fields can be calculated easily.

Main problem with this method is the large programming effort required to get to the result. In a similar pattern, we have other semi-empirical methods like surface current model, hankel transform method, reciprocity method, GEBC Technique etc.

As we saw Cavity model is good for basic MPA geometry, but whenever the design deviates from this basic,like thick patch, dielectric cover, multiple layers, shortening wall, shortening pins, slots etc., its explanation and prediction of result become difficult. In addition to this, even for thin substrate it relies on results found experimentally, to account for the fringing fields. Using proximity fee, aperture coupled feed, extension to

stripline feed further complicates the problem.

3.4 Full Wave Analysis

All these above mentioned cases can ne solved by solving the Maxwell's equation, satisfying the boundary conditions. This approach is called Full Wave Analysis. This approach can be further divided into two methods:

1. Method of Moments.
2. Finite Difference time domain.

3.4.1 MOM

Formulation of the problem is done in the form of integral equations, taking magnetic and electrical currents as unknown variables. Let us take the example of a superstrate, which is a dielectric layer above the patch of MPA. This problem can not be analysed using cavity model. Pozar [46], Fan *et. al.* [47] have made significant contribution in this topic. This analysis for the above mentioned case goes in following steps:

1. Coaxial cable can be modeled as cylindrical uniform current sheet with radius a_ρ
2. For different regions like superstrate, substrate, and air, wave equation solutions are obtained in the domain of Fourier transform.
3. Apply boundary conditions across interfaces, ground plane, and at infinity, to obtain arbitrary coefficients.
4. For unknown surface current density on the patch, integral equations are obtained by enforcing condition of no tangential electric field presence on the patch.
5. To solve surface current density, Galerkin's method is used.
6. Calculations of resonant frequency, field pattern, and input impedances is done.

Fourier transform in two dimension, of function $f(x,y)$ is taken as $\tilde{f}(k_x,k_y)$, given by by:

$$\tilde{f}(k_x,k_y) = \iint f(x,y)e^{j(k_x x+k_y y)}\mathrm{d}x\mathrm{d}y \tag{3.35}$$

$$f(x,y) = \frac{1}{4\pi^2}\iint \tilde{f}(k_x,k_y)e^{-j(k_x x+k_y y)}\mathrm{d}k_x\mathrm{d}k_y \tag{3.36}$$

If we denote electric field in air, superstrate, substrate regions by $\vec{E_0},\vec{E_1},\vec{E_2}$ and then satisfying the wave equations:

$$\nabla^2\vec{E_0} + {k_0}^2\vec{E_0} = 0, \quad \text{(air)} \tag{3.37}$$

$$\nabla^2\vec{E_1} + \epsilon_{r1}{k_0}^2\vec{E_1} = 0, \quad \text{(superstrate)} \tag{3.38}$$

$$\nabla^2\vec{E_2} + \epsilon_{r2}{k_0}^2\vec{E_2} = j\omega\mu_0\vec{J_p}, \quad \text{(substrate)} \tag{3.39}$$

where,

$$\vec{J_p} = \hat{z}J_p(x,y) \tag{3.40}$$

$$= \hat{z}\frac{I_0}{2\pi}\frac{\delta[|\vec{r}-\vec{r_p}|-a_p]}{|\vec{r}-\vec{r_p}|} \tag{3.41}$$

$$|\vec{r}=\vec{r_p}| = \sqrt{(x-x_p)^2+(y-y_p)^2} \tag{3.42}$$

If we assume both the superstrate and substrate to be infinite in xy plane, the fourier transformed equations become:

$$\Big(\frac{\partial^2}{\partial z^2}+{\gamma_0}^2\Big)\tilde{E}_0(k_x,k_y,z) = 0, \quad \text{(air)} \tag{3.43}$$

$$\Big(\frac{\partial^2}{\partial z^2}+{\gamma_1}^2\Big)\tilde{E}_1(k_x,k_y,z) = 0, \quad \text{(superstrate)} \tag{3.44}$$

$$\Big(\frac{\partial^2}{\partial z^2}+{\gamma_2}^2\Big)\tilde{E}_2(k_x,k_y,z) = j\omega\mu_0\hat{z}\tilde{J}_p(k_x,k_y), \quad \text{(substrate)} \tag{3.45}$$

where,

$$k_t{}^2 = k_x{}^2 + k_y{}^2 \tag{3.46}$$

$$\gamma_i = \sqrt{\epsilon_{ri} k_0{}^2 - k_t{}^2} \quad i = 0, 1, 2 \tag{3.47}$$

Solution to equation 3.37-3.39 are:

$$\tilde{E}_0(k_x, k_y, z) = \vec{A}_0 e^{-j\gamma_0(z-d_1-d_2)}, \text{ (air)} \tag{3.48}$$

$$\tilde{E}_1(k_x, k_y, z) = \vec{A}_1 e^{-j\gamma_1(z-d_2)} + \vec{B}_1 e^{-j\gamma_1(z-d_2)}, \text{ (superstrate)} \tag{3.49}$$

$$\tilde{E}_2(k_x, k_y, z) = \vec{A}_2 e^{-j\gamma_2(z-d_2)} + \vec{B}_2 e^{-j\gamma_2(z-d_2)} + \frac{j\omega\mu_0 \tilde{J}_p \hat{z}}{\gamma_2{}^2}, \text{ (substrate)} \tag{3.50}$$

We have following interface equations:

$$\hat{z} \times \vec{E}_2 = 0, \quad z = 0 \tag{3.51}$$

$$\hat{z} \times (\vec{E}_1 - \vec{E}_2) = 0, \quad z = d_2 \tag{3.52}$$

$$\hat{z} \times (\vec{H}_1 - \vec{H}_2) = \vec{J}_s, \quad z = d_2 \tag{3.53}$$

$$\hat{z} \times (\vec{E}_0 - \vec{E}_1) = 0, \quad z = d_1 + d_2 \tag{3.54}$$

$$\hat{z} \times (\vec{H}_0 - \vec{H}_1) = 0, \quad z = d_1 + d_2 \tag{3.55}$$

$$\tag{3.56}$$

Solving all these equations, which is a lengthy process, gives us E_{2x}, E_{2y} in the form of double integral equations, which are then solved using Galerkin's Method. In Galerkin's method, we expand the surface currents (unknown) in series of domain basis functions as:

$$J_{sx}(x, y) = \sum_{n=1}^{N_x} C_{xn} J_{sxn}(x, y) \tag{3.57}$$

$$J_{sy}(x, y) = \sum_{n=1}^{N_y} C_{yn} J_{syn}(x, y) \tag{3.58}$$

with,

$$J_{sxn} = \sin\frac{k\pi}{a}\left(x+\frac{a}{2}\right)\cos\frac{l\pi}{b}\left(y+\frac{b}{2}\right) \tag{3.59}$$

$$J_{syn} = \cos\frac{k\pi}{a}\left(x+\frac{a}{2}\right)\sin\frac{l\pi}{b}\left(y+\frac{b}{2}\right) \tag{3.60}$$

where n denotes various a,k combinations. In equation **??** and next, we have written J_{sx}, and J_{sy}. Their Fourier transform may be written as:

$$\tilde{J}_{sx}(k_x,k_y) = \sum_{n=1}^{N_x} C_{xn}\tilde{J}_{sxn}(k_x,k_y) \tag{3.61}$$

$$\tilde{J}_{sy}(k_x,k_y) = \sum_{n=1}^{N_y} C_{yn}\tilde{J}_{syn}(k_x,k_y) \tag{3.62}$$

For the case of no superstrate, we can take $d = 0$, that is we can easily get the results for simple MPA, from the results obtained using above method. Presence of superstrate also decreases the resonant frequency. With this method, we can also analyze not only rectangular MPA but also the annular or the circular one, also different types of feeds can be properly incorporated with this method.

3.4.2 FDTD

Maxwell's equations, present in differential form are converted into difference equation and are then solved, this method is called FDTD. Yee [48] first proposed this method for solving EMW equations. As compared to the methods depending on frequency domain, this method needs more time and memory, but this method is more reliable for the cases of very complex antenna structures. With this method, we can find the complete frequency response, just with a single simulation.

Yee algorithm

Two of the Maxwell's equations for the case of a homogeneous, linear, isotropic and non dispersive medium can be written as:

$$\nabla \times \vec{E} = -\mu \frac{\partial \vec{H}}{\partial t} - \rho^* \vec{H} \tag{3.63}$$

$$\nabla \times \vec{H} = -\epsilon \frac{\partial \vec{E}}{\partial t} + \sigma \vec{E} \tag{3.64}$$

where σ and ϵ are conductivity, permittivity, and ρ^* and μ are resistivity and magnetic permeability of the medium.

Rearranging equations 3.63 and 3.64, and applying them on a rectangular coordinate system, we get:

$$\frac{\partial H_x}{\partial t} = \frac{1}{\mu}\Big(\frac{\partial E_y}{\partial z} - \frac{\partial E_z}{\partial y} - \rho^* H_x\Big) \tag{3.65}$$

$$\frac{\partial H_z}{\partial t} = \frac{1}{\mu}\Big(\frac{\partial E_x}{\partial x} - \frac{\partial E_y}{\partial z} - \rho^* H_z\Big) \tag{3.66}$$

$$\frac{\partial H_y}{\partial t} = \frac{1}{\mu}\Big(\frac{\partial E_z}{\partial x} - \frac{\partial E_x}{\partial z} - \rho^* H_y\Big) \tag{3.67}$$

$$\frac{\partial E_x}{\partial t} = \frac{1}{\epsilon}\Big(\frac{\partial H_z}{\partial y} - \frac{\partial H_y}{\partial z} - \sigma E_x\Big) \tag{3.68}$$

$$\frac{\partial E_z}{\partial t} = \frac{1}{\epsilon}\Big(\frac{\partial H_y}{\partial x} - \frac{\partial H_x}{\partial y} - \sigma E_z\Big) \tag{3.69}$$

$$\frac{\partial E_y}{\partial t} = \frac{1}{\epsilon}\Big(\frac{\partial H_x}{\partial z} - \frac{\partial H_z}{\partial x} - \sigma E_y\Big) \tag{3.70}$$

In this method we define, a Yee [48] cell, which is just a discretization of the problem space. With this small rectangular cell, we discretizes x, y, z domain, as shown in Figure 3.6 and we also discretizes the time domain, for using this method. In the domain of space, and time, a field component can be written as:

$$F^n(i,j,k) = F(i \triangle_x, j \triangle_y, k \triangle_z, n \triangle t) \tag{3.71}$$

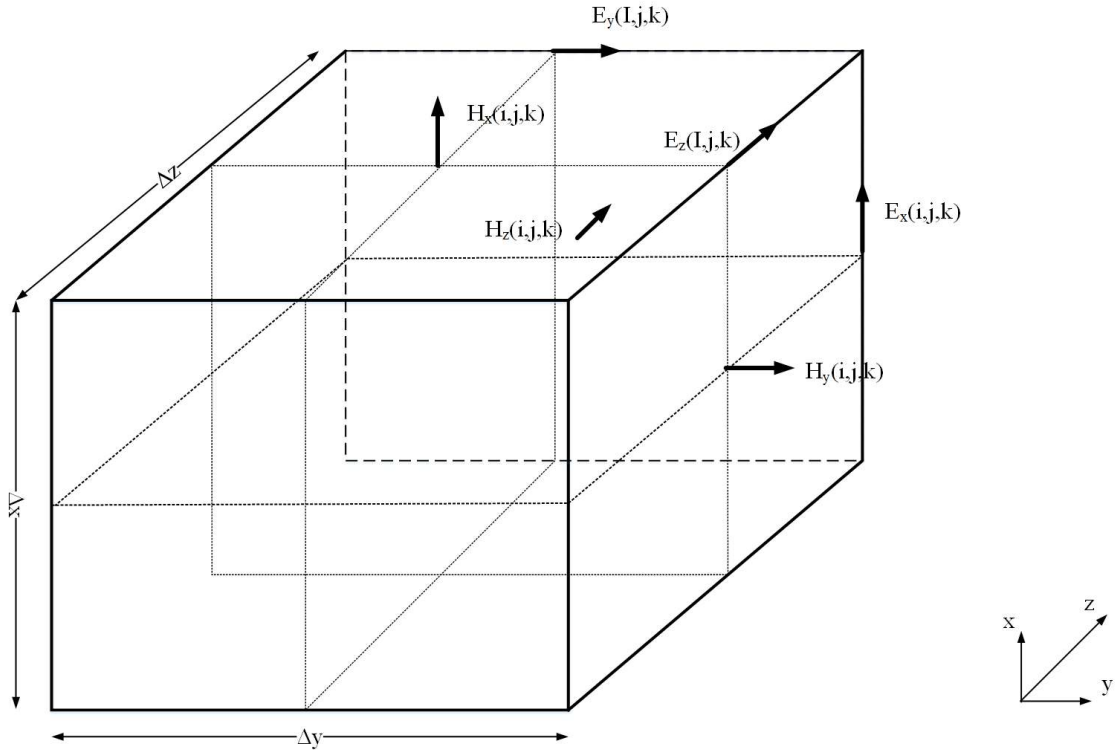

Figure 3.6: Yee cell used in FDTD

where discretization steps along x, y, and z are denoted by $\triangle\, x$, $\triangle\, y$, and $\triangle\, z$, whereas n denotes the time step. Taking derivatives of equation 3.71, and approximating using central difference method:

$$\frac{\partial F^n(i,j,k)}{\partial x} = \frac{F^n(i+1/2,j,k) - F^n(i-1/2,j,k)}{\triangle\, x} \tag{3.72}$$

$$\frac{\partial F^n(i,j,k)}{\partial t} = \frac{F^{n+1/2}(i,j,k) - F^{n-1/2}(i,j,k)}{\triangle\, t} \tag{3.73}$$

which possess a good accuracy upto the second order of *vartrianglet*, and *vartrianglex*. After this, the solution is forwarded using Lee's algorithm Leap-Frog.

Other points to be taken in mind, regarding this method are, size of Yee cell should be small enough, below $1/10^{th}$ of the lowest wavelength present, that is concerning for the highest frequency present. Also the step in time should also be appropriate, in accordance to maintain the stability, which is given by the stability criteria given by

Courant:

$$v_{max} \cdot \triangle\, t \leq \frac{1}{\sqrt{(1/\triangle\, x)^2 + (1/\triangle\, y)^2 + (1/\triangle\, z)^2}} \tag{3.74}$$

where v_{max} denotes highest velocity of propagating wave, present in the problem domain, which is usually the spped of light. This gives us the maximum allowed time step. Yee cells are defined such that, if their exist a change in material, then it is good to have wall of the Yee cell on the boundary. Some of the parameters like permittivity are average on these boundaries ,thus modifying the equation **??**, **??**, assuming interface on y-z plane,

$$\frac{\epsilon_1 + \epsilon_2}{2} \cdot \frac{\partial E_y}{\partial t} = \frac{\partial H_x}{\partial z} - \frac{\partial H_z}{\partial x} - \sigma E_y \tag{3.75}$$

$$\frac{\epsilon_1 + \epsilon_2}{2} \cdot \frac{\partial E_z}{\partial t} = \frac{\partial H_y}{\partial x} - \frac{\partial H_x}{\partial y} - \sigma E_z \tag{3.76}$$

whereas, if boundary is non magnetic, their is not need for updation for values of μ, as it remains continuous. Accurate ABC should be used, as a good boundary condition for absorption of waves, as no computer can implement an infinite space, it has to properly truncate the to some limit.

Chapter 4

Antenna Arrays

4.1 Introduction to arrays

4.1.1 Concept of arrays

Usually radiation pattern from a single antenna element is very wide with a low directivity. In that case, to increase the directivity of antenna, it is required to increase its electrical length. Another method to increase the electrical length or directivity of an antenna system is to use multi element arrays [49]. In most of the cases, all the elements of an array are same, although there is no such compulsion. Total field is obtained by doing vector addition of fields from individual antenna element. Direction in which, the fields interfere constructively produced have good directivity in that direction, whereas a destructive interference in a direction cause a reduced total field in that direction.
For the antenna arrays [50] with identical elements, we have following control elements to control the overall field produced:

1. Overall array geometrical configuration.

2. Displacement between elements.

3. Amplitude of excitation of individual elements.

4. Phase of excitation of individual elements.

5. Individual elements' relative pattern.

4.2 Basic two element array

Consider two horizontal infinitesimal dipoles [50] placed along the z-axis, shown in Figure 4.1 (a). The total radiated field by the two elements, considering no mutual coupling

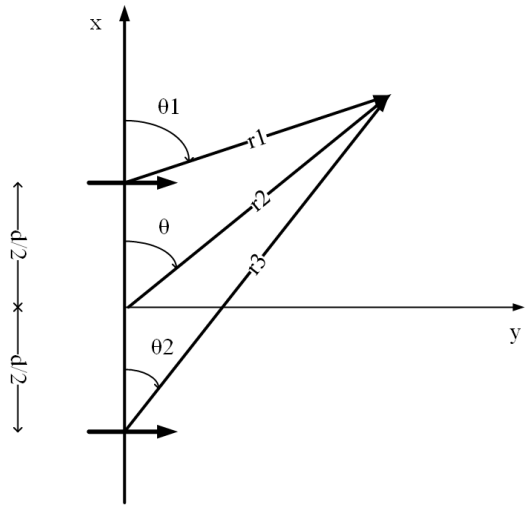

(a)

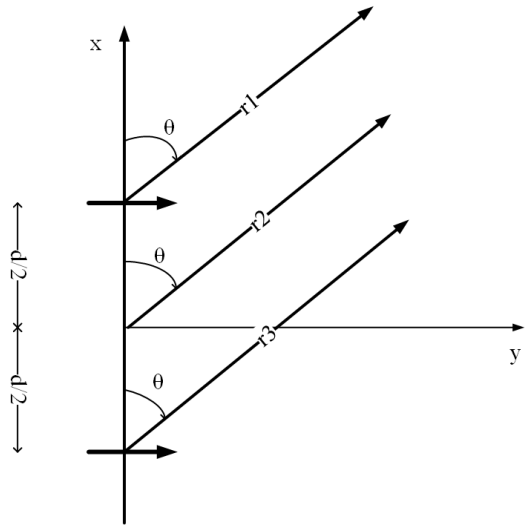

(b)

Figure 4.1: (a) Two element array. (b) Far-field observation.

between them is simply the vector sum of radiated field by two elements, given by:

$$\begin{aligned} \mathbf{E}_t &= \mathbf{E}_1 + \mathbf{E}_2 && (4.1) \\ &= \hat{\mathbf{a}}_\theta j\eta \frac{kI_0 l}{4\pi} \left\{ \frac{e^{-j[kr_1-(\beta/2)]}}{r_1} \cos\theta_1 + \frac{e^{-j[kr_2-(\beta/2)]}}{r_2} \cos\theta_2 \right\} && (4.2) \end{aligned}$$

where β is difference in excited phase between elements. Magnitude excitation is considered identical. Doing approximation for the far field, as shown in Figure 4.1 (b) gives,

$$\begin{aligned} \theta_1 &\simeq \theta_2 \simeq \theta && (4.3) \\ r_1 &\simeq r - \frac{d}{2}\cos\theta \ \text{ for variation in phase} && (4.4) \\ r_2 &\simeq r + \frac{d}{2}\cos\theta \ \text{ for variation in phase} && (4.5) \\ r_1 &\simeq r_2 \simeq r \ \text{ for variation in amplitude} && (4.6) \end{aligned}$$

So, the equation 4.1 can be modified to

$$\begin{aligned} \mathbf{E}_t &= \hat{\mathbf{a}}_\theta j\eta \frac{kI_0 l e^{-jkr}}{4\pi r} \cos\theta \left[e^{+j(kd\cos\theta+\beta)/2} + e^{-j(kd\cos\theta+\beta)/2} \right] && (4.7) \\ &= \hat{\mathbf{a}}_\theta j\eta \frac{kI_0 l e^{-jkr}}{4\pi r} \cos\theta \left\{ 2\cos\left[\frac{1}{2}(kd\cos\theta+\beta) \right] \right\} && (4.8) \end{aligned}$$

We can easily see that the total field produced by the antenna system is product of the field produced by a single element place at the origin with the array factor. This gives the array factor,

$$AF = 2\cos[\frac{1}{2}(kd\cos\theta+\beta)] \qquad (4.9)$$

that is,

$$\mathbf{E}(\text{total}) = [\mathbf{E}(\text{single element on reference point})] \times [\text{array factor}] \qquad (4.10)$$

This array factor, depends upon geometry of antenna system and the phase of excitation.

4.3 Feeding Network in Linear Arrays

4.3.1 Series Feed

In series-feed[51] , connection between the radiating elements is in series through a uniform transmission line, as shown in Figure 4.2. Mainly we have two types of series-fed

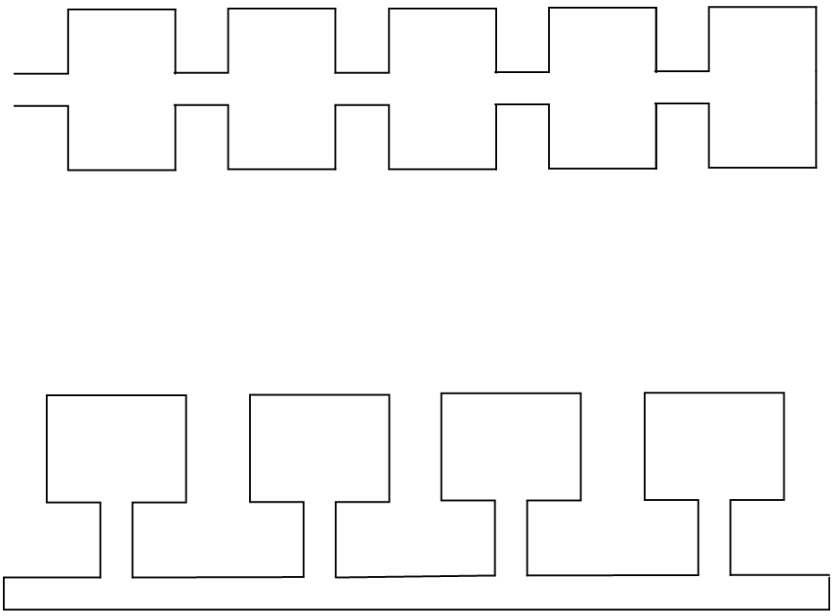

Figure 4.2: Linear array series fed

arrays.

Traveling wave array

Matching of impedance of transmission line and radiating elements is done here, Spacing between the elements play a very important role of providing the proper phases. Since the wave is a traveling wave on transmission line, energy decays as it progresses. A properly matched element can be used at the end of the array to absorb the remaining energy. The limitation of traveling wave array is that the beam shifts with change in frequency.

Resonant Series fed

In Resonant series fed type of arrays, focus is not on matching of feed point and the antenna, but enhanced focus is given on the spacing between the elements. Bouncing wave because of improper matching at the feed point also causes radiation helping the system to get a better broadside pattern, but the insertion loss is higher.

4.3.2 Parallel Feed

In parallel or corporate feed, all the elements of the array are fed with same power and same phase, as shown in Figure 4.3. The feed line is kept divided until it reach all the

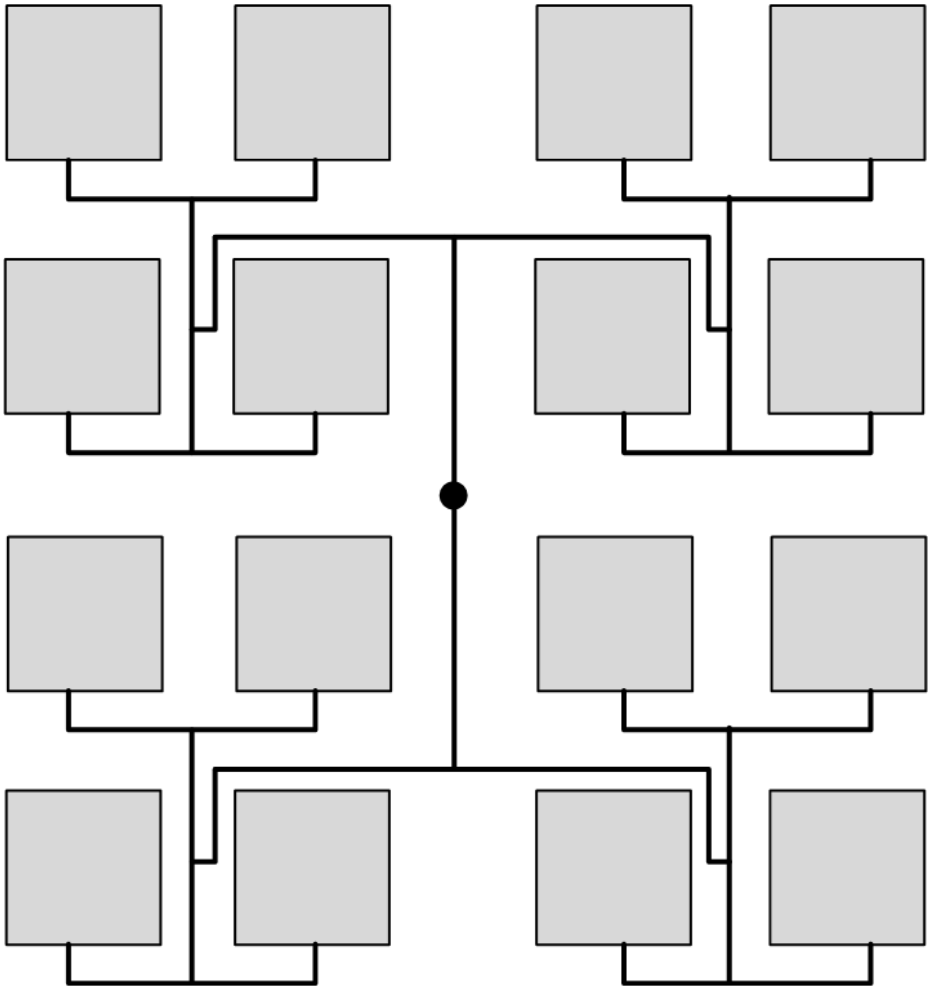

Figure 4.3: Two dimensional Parallel fed array

elements, thus dividing the power equally, and since the length of the line reaching each element is same, so the phase is also same. Disadvantage is a big structure, also large number of distributaries can lead to higher insertion loss.

4.3.3 Parallel and Series

Both series fed and parallel fed have their own advantages and disadvantages individually. It is on the designer, ho he/she manipulates them. Figure 4.4 shows two rows of antenna

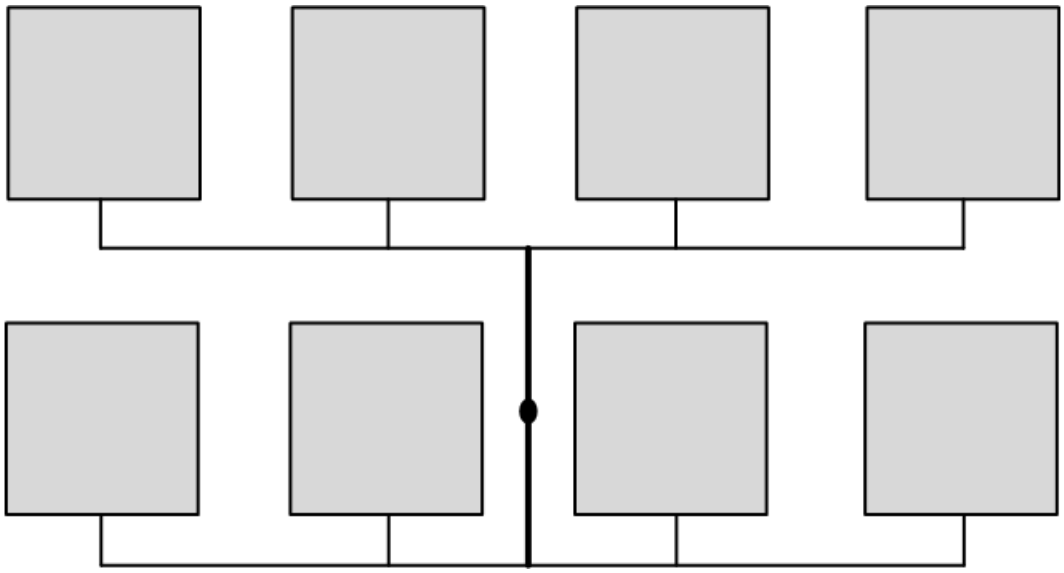

Figure 4.4: Parallel-Series two dimensional array

arrays which are connected in parallel, but within each row, elements are connected in series. We can obtain a broadside pattern with this configuration.

4.3.4 Anti Phase Technique

J. Huang [52] [52] proposed this method. In this method, opposite excitation is provided to subsets of the array such that higher mode unwanted cross polar radiations are alleviated, as shown in Figure 4.5. Also, usually the upper row is inverted. Half wave transformer is used for proper phasing.

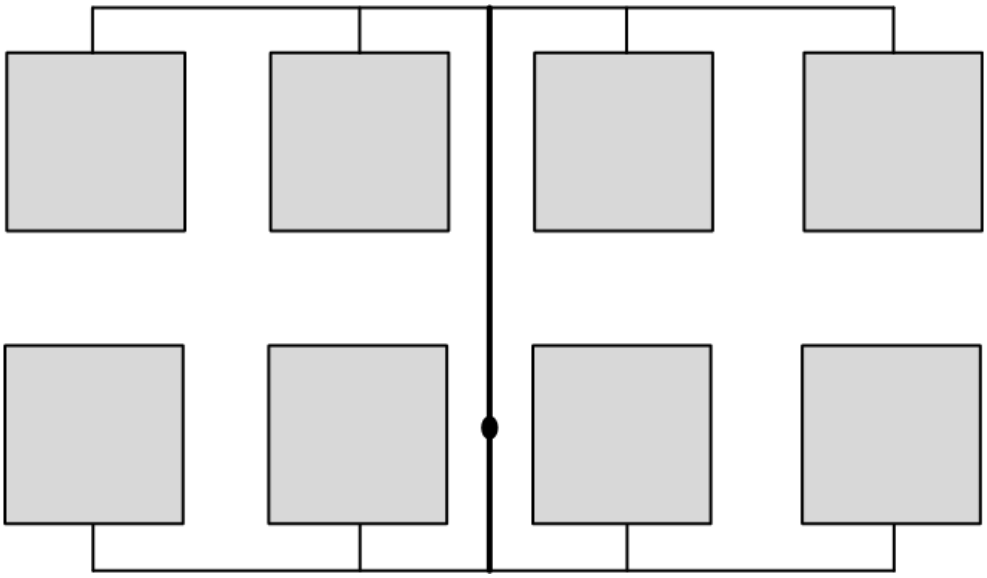

Figure 4.5: Anti-Phase array

Chapter 5

Designs, Results, and Discussions

A full-wave simulator, specialized in Electromagnetic simulations at high frequency, CST Microwave Studio® 2014 [16] has been used for all simulation work in this thesis. This simulation software work on a numerical method called Finite Integration Technique (FIT) [53], which discretizes the below mentioned Maxwell's equations [54] in integral form instead of differential ones,

$$\oint \mathbf{E} \cdot \mathrm{d}\mathbf{L} = -\int_S \frac{\partial \mathbf{B}}{\partial t} \cdot \mathrm{d}\mathbf{S} \tag{5.1}$$

$$\oint \mathbf{H} \cdot \mathrm{d}\mathbf{L} = \int_S \left(\mathbf{J} + \frac{\partial \mathbf{D}}{\partial t} \right) \cdot \mathrm{d}\mathbf{S} \tag{5.2}$$

$$\oint_S \mathbf{D} \cdot \mathrm{d}\mathbf{S} = \int_{vol} \rho_v \mathrm{d}v \tag{5.3}$$

$$\oint_S \mathbf{B} \cdot \mathrm{d}\mathbf{S} = 0 \tag{5.4}$$

where $\mathbf{D}$ is Electric flux density, $\mathbf{E}$ is Electric Field Intensity, $\mathbf{B}$ is Magnetic Flux Density, $\mathbf{H}$ is Magnetic Field Intensity, $\mathbf{J}$ is conduction current density, ρ_v is volume charge density and $\mathrm{d}\mathbf{L}, \mathrm{d}\mathbf{S}, \mathrm{d}v$ are differential length, surface area, volume respectively. This software breaks the calculation domain in small cuboidal cells, and solves the maxwell equations on all of its facets (boundaries).

The fabrication part has been done by Ariens India Private Limited, Phase-8, Industrial

Area, Mohali, Punjab; and for testing work, NITTTR, Sector-26, Chandigarh have been approached along with the Antenna Research Laboratory present in our college.

5.1 MPA with CSRRs and RIS

In the design shown in Figure 5.1 a MPA loaded with a pair of CSRRs [55] oriented face to back are shown, the structure is mainly a stalked structure. A layer of RIS [56]

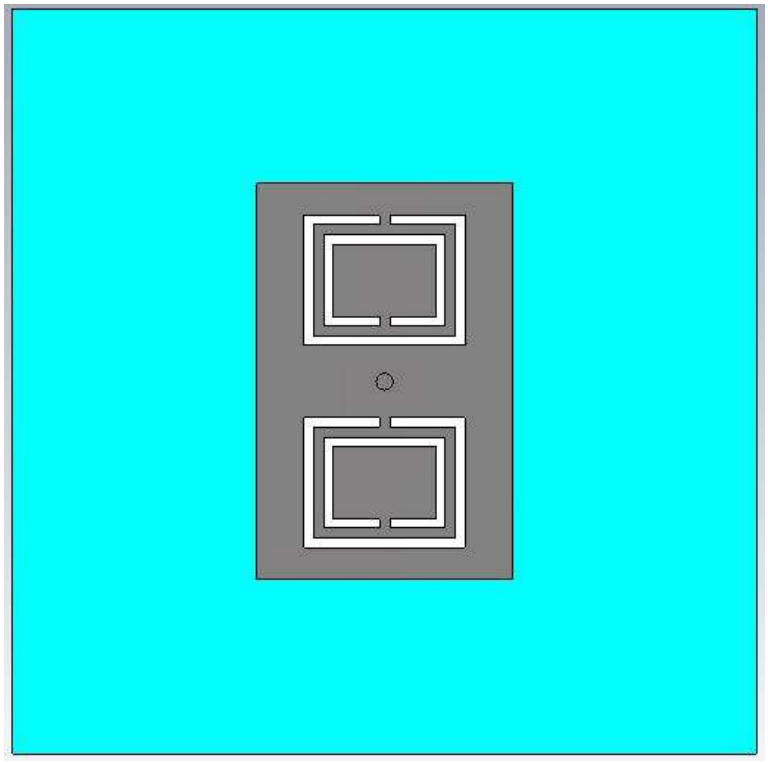

Figure 5.1: MPA loaded with CSRRs oriented face to back

has been sandwiched inside the substrate. Layer by layer stacking of various elements involved is shown in Figure 5.2 and 5.3 The lower most layer is ground, which is a metal (copper), over this layer we have a substrate "MEGTRON 6", relative permittivity 4.02 and loss tangent .009 at 2.4 GHz. Thickness of this substrate is 2.6 mm. Above this we an EBG structure in the form of RIS, which is a meta-material with periodic mettalic structures. Above this we again have the same substrate but with 0.4 mm height. Above this we have the metallic patch in which the slots have been cut to form two pairs of

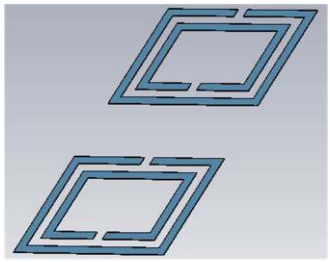

(a) CSRRs

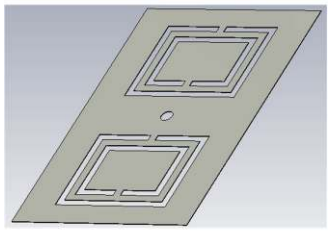

(b) Metallic Patch

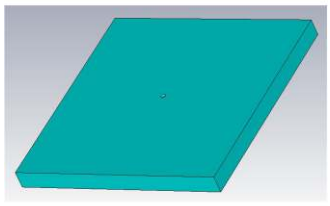

(c) Substrate-upper layer

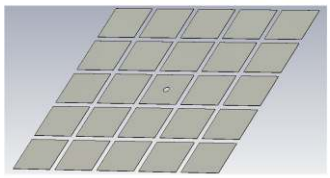

(d) RIS

Figure 5.2: Layer by layer structure of MPA with CSRRs and RIS

CSRRs. The feed used is a coaxial feed, fed in the middle of the patch, which have the a inner conductor covered by a dielectric material, which is again covered by a conductor in cylindrical shape, which is connected to ground. Mesh used is finer at locations where cell density is high, as shown in Figure 5.4 As we kept on making the mesh more finer, with each pass, the accuracy of results increases. Figure 5.5 shows the $|S_{11}|$ dB curve for the above mentioned design, where $|S_{11}|$ is the scattering parameter which tells us how much power is reflected back to same port, from which it is delivered (we have used only one port here). This curve shows that by making mesh more finer with each pass, our frequency of radiation converges towards 2.4 GHz, with lower return loss. This

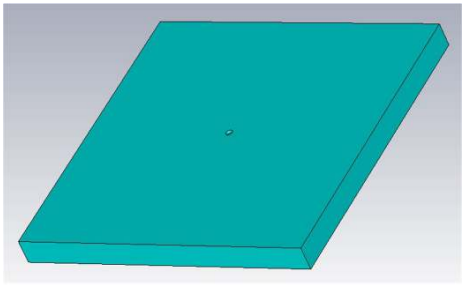

(e) substrate- lower layer

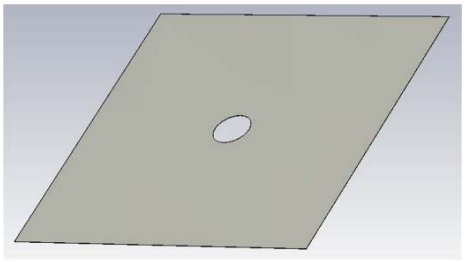

(f) metallic ground

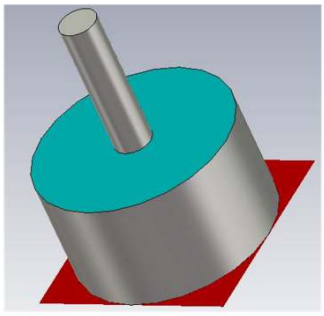

(g) coaxial feed

Figure 5.3: Layer by layer structure of MPA with CSRRs and RIS continued

configuration is showing only a single band of operation or the antenna is radiating only at 2.4 GHz.

Next a right shift 2.8 mm is done in the feed location, as shown in Figure 5.6 and again the $|S_{11}|$ dB plot is observed. Just with the shift in the location of coaxial feed, we now have dual band antenna, one resonating frequency around 2.4 GHz and another around 3.75 GHz.

Next the configuration of CSRRs is changed to side by side and the coaxial feed is shift to left, 2.8 mm left to center of the patch. With this configuration we have added one more radiating band, thus getting a triple band antenna, radiating at 2.25 GHz, 2.55

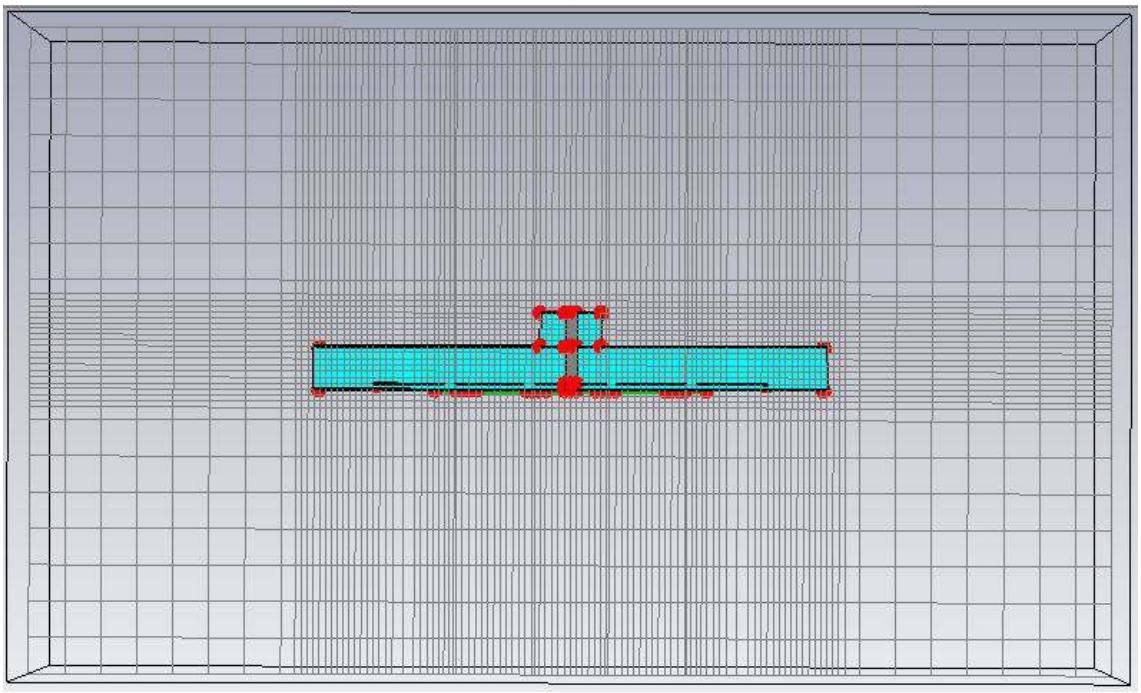

Figure 5.4: Finer mesh at high density areas

GHz, and 3.58 GHz, as shown in Figure 5.7. With this, it can easily be observed that just with the change in the configuration of CSRRs or feed location, we can get single band antenna, dual band antenna, or triple band antenna as required, in accordance with the application. This shows the versatility added to the design using CSRRs.

5.2 Dual Band Stepped-Impedance Array Loaded with CSRRs

A suspended dual band planar antenna based on a stepped-impedance structure modified to an array, loaded with Complementary Split-Ring Resonators (CSRRs), possessing good directivity pertaining point to point backhaul communication is acquainted. The presented antenna radiates at 2.4-2.5 GHz (4.4%) and 5.3-5.9 GHz (12%) with $|S_{11}| < -10$ dB, accompanying directivity of 11.6 dBi and 11.3 dBi respectively. The antenna is loaded with CSRRs which works as a L-C tank resonator, to obtain better coupling, and to lower the frequency of radiation in 2.4 GHz band along with decreasing

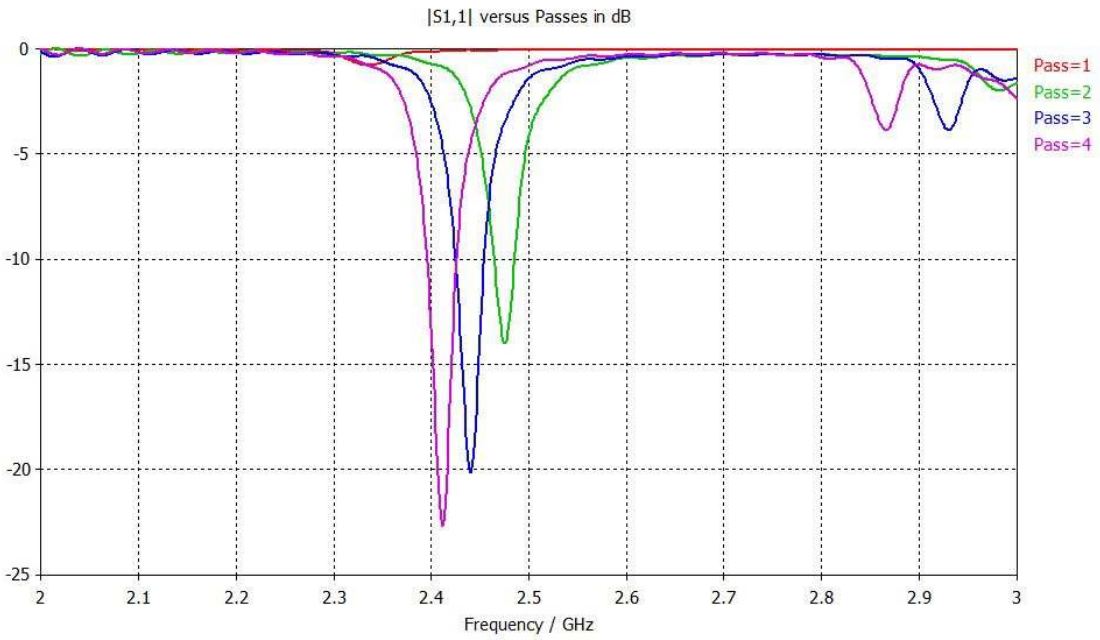

Figure 5.5: Single band antenna, $|S_{11}|$ dB curve with increasing density of mesh cells

the return loss for both the bands of WLAN. The Suspended antenna, symmetrical across vertical axis, has four branches, each of which are obtained from Maximally Stepped-Impedance filter. A stable radiation pattern with high directivity in both the WLAN bands is achieved.

5.2.1 Design methodology

While designing this microstrip patch antenna, following problems have been taken into consideration:

1. Overlapping of radiation of individually placed antennas for 2.4 GHz and 5.5 GHz, the presence of coupling between them results in reduction in radiation efficiency.

2. Electrical length of antennas (for 2.4 GHz & 5.5 GHz) are different, this 2.4 GHz radiator has large electrical length at 5.5 GHz, higher order modes from 5.5 GHz resonances with 2.4 GHz radiation, giving out unwanted radiation patterns.

3. Separate single port feeding is required for each radiating antenna.

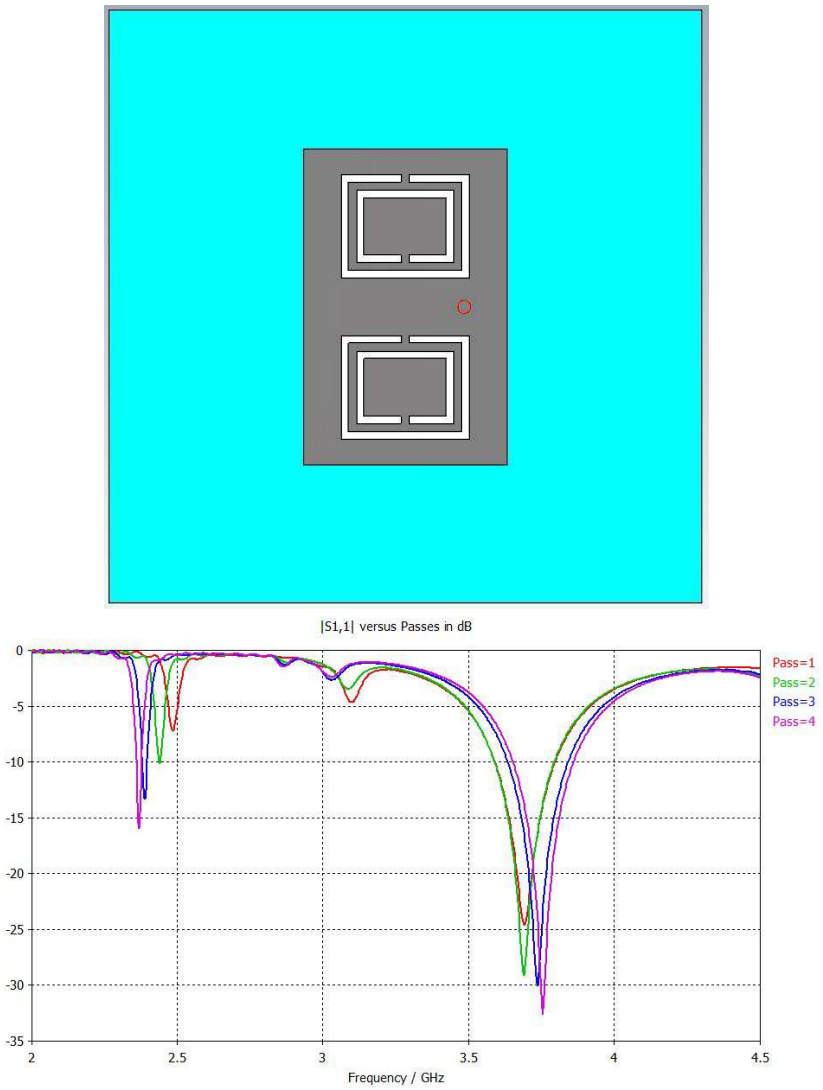

Figure 5.6: Dual band antenna, design and result for feed shift to right by 2.8 mm

4. Directivity of the antenna should be high.

5. Material costs should be low, so that the antenna can be easily used commercially.

The proposed solutions implemented in the design are as follows:

1. Series fed network is used, reducing the count of microstrip lines, minimizing the unwanted mutual coupling between various feeding networks and radiators. Also Split Ring Resonators (SRRs) are employed to manipulate the coupling further.

2. Microstrip Stepped-Impedance low pass filter is used such that it has a passband

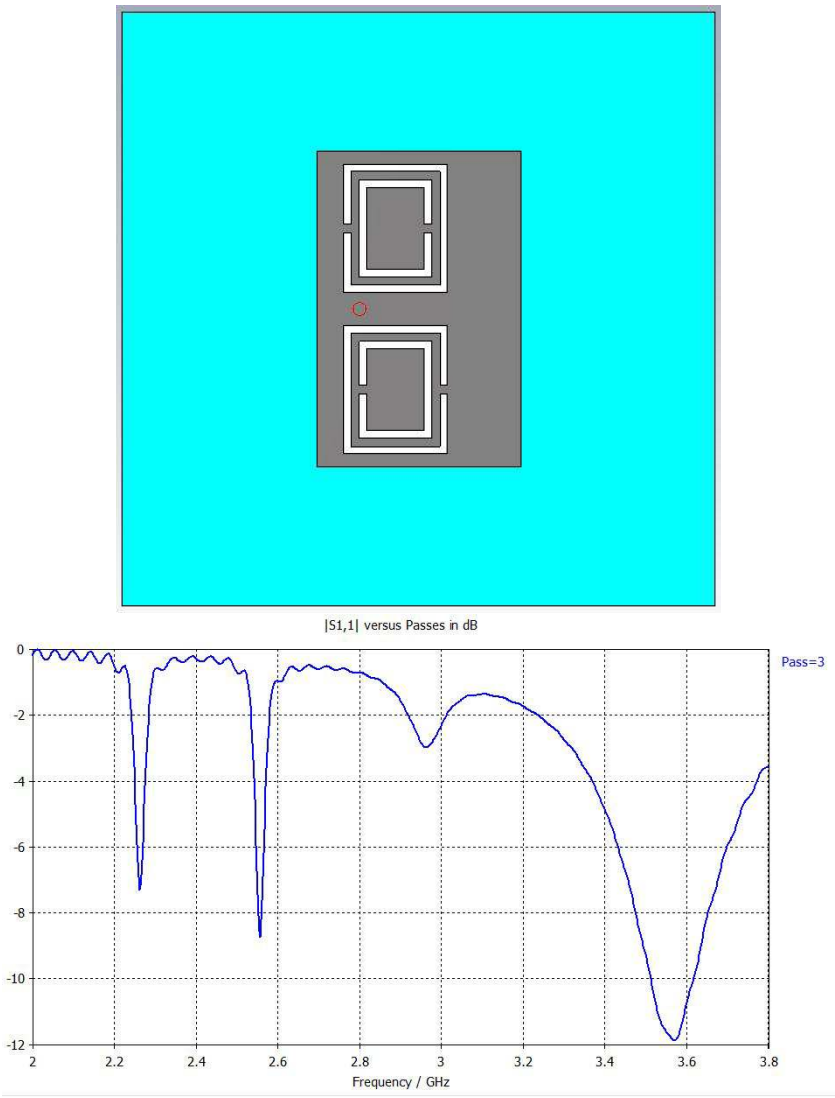

Figure 5.7: Triple band antenna, design and result for feed shift to right by 2.8 mm

over 2.4 GHz and stopband over 5.5 GHz, to excite the 2.4 GHz radiator. This avoids 2.4 GHz radiations from showing resonance in 5.5 GHz band. This hi-Z low-Z low pass filter is easy to design and occupy less space than that used with stubs, but this does not produce a sharp attenuation, which is not needed here as both the bands are not consecutive but far apart.

3. Signals are reflected through resonators, and then radiated again. Better impedance matching is employed, adding more control over parameters through Split Ring Resonators.

Table 5.1: Maximally Flat Low-Pass Filter Prototype Element Values

N	g_1	g_2	g_3	g_4	g_5
1	2.0000	1.0000			
2	1.4142	1.4142	1.0000		
3	1.0000	2.0000	1.0000	1.0000	
4	0.7654	1.8478	1.8478	0.7654	1.0000

4. For better directivity, design is a modification over an array [57], where arrays are always known to enhance the directivity.

5. This design is a suspended patch antenna design, thus air is used as a substitute for substrate material, So that the material cost for substrate is very less, which can play a big role in commercial use.

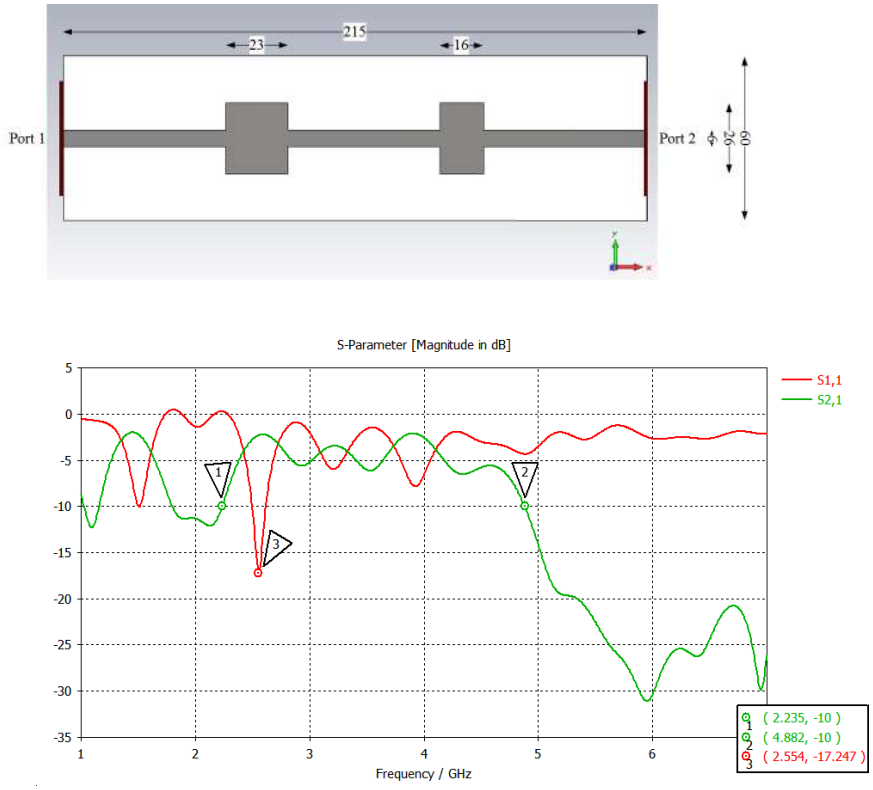

Figure 5.8: (a) Stepped-Impedance Low Pass Filter design. (b) S-Parameters

Using Table 5.1 [58], taking 2nd order filter with $N = 2$, $C_1 = 1.4142$, $L_2 = 1.4142$, $C_3 = 1.0000$, Step-Impedance [59] Microstrip Low-pass filter with pass-band in the 2.4 GHz band along with stop-band in 5 GHz band, possessing a low return loss around 2.5 GHz is depicted in Figure 5.8. A high high-low impedance ratio is used, for better approximations. Half of the filter, shown in Figure 5.8 is 180° rotated, and the dimensions of lower and higher impedance lines are changed, and configured as an array structure as shown in Figure 5.9 to obtain radiation in 2.4, 5 GHz bands. Figure 5.9 shows the

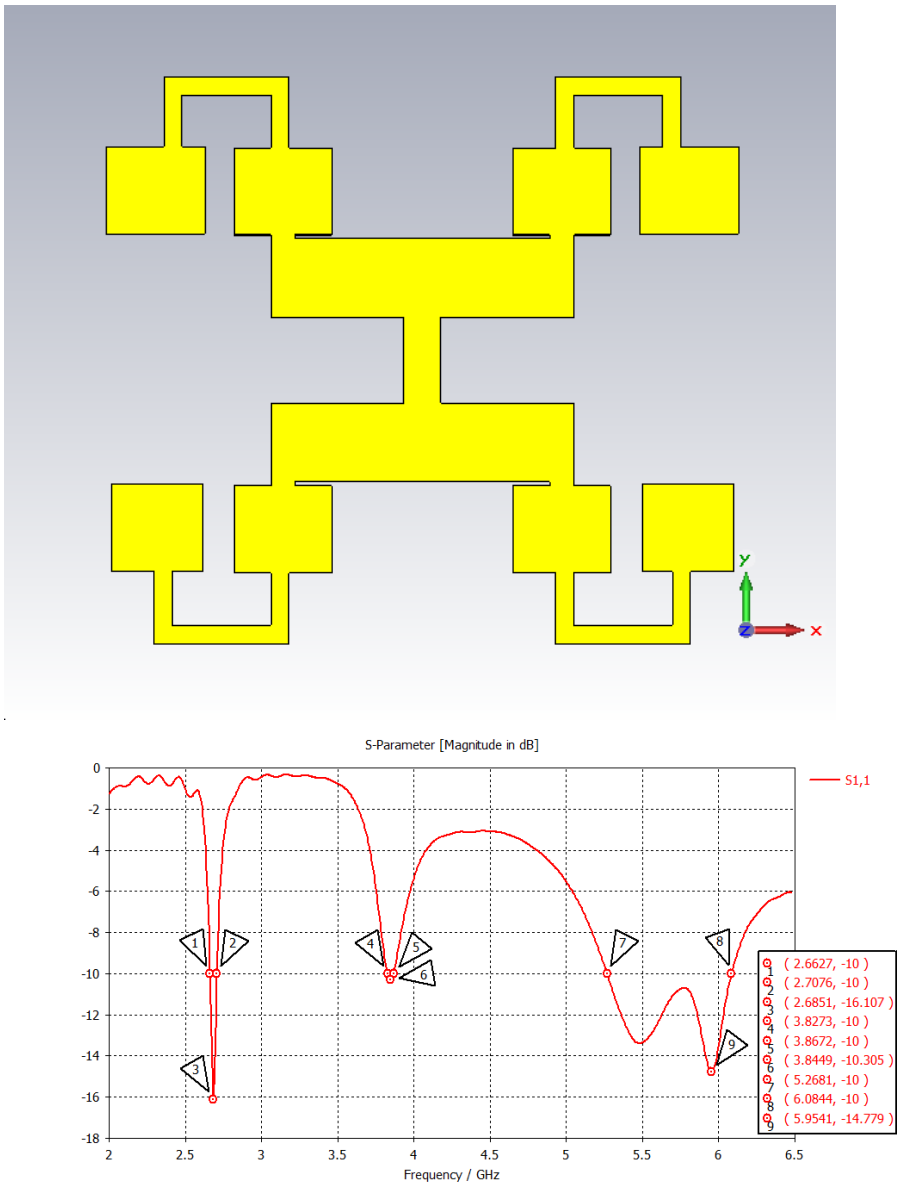

Figure 5.9: (a) Planar array design without CSRRs. (b) Reflection Coefficient.

planar antenna array obtained from modifications in stepped-impedance structure, it shows three possible bands of radiations, around 2.69 GHz, 3.85 GHz, and 5.5 GHz. The first band needs to be shifted towards lower frequency, and the middle one is unwanted as it will reduce the radiation aperture for the two bands of WLAN network. These two problems, as well as lower return loss at required frequency bands will be obtained by incorporating this design with CSRRs, which are discussed in following sections. CSRRs

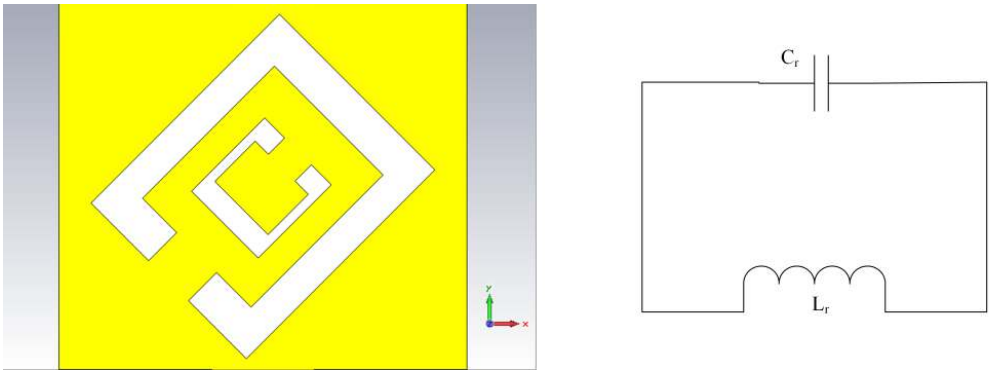

Figure 5.10: CSRR and its equivalent circuit

exhibit negative permittivity [60]. Here it works mainly as a resonator instead of a radiator, providing more control over the coupling. It acts like a tank L-C Resonator circuit [61] as shown in Figure 5.10. The Capacitive coupling is mainly obtained from ring slots, while the outer ring's split provides magnetic coupling.

5.2.2 Design

Figure 5.11 shows the planar antenna array loaded with Complementary Split Ring Resonators. This design is symmetrical across y-axis, giving symmetrical radiation in H-plane. The structure is suspended above the ground plane of size 185 × 170, at the height of 1 mm. All the measurements and angles have been depicted in the Figure itself. Stepped-Impedance structure is used and modified as an array, for better directivity; which radiated in 2.5 GHz, 5 GHz bands, in addition to an unwanted band. This shortcoming was removed by using CSRRs, which act as a resonator providing more maneuverability over mutual coupling, it also results in better reflection coefficients in

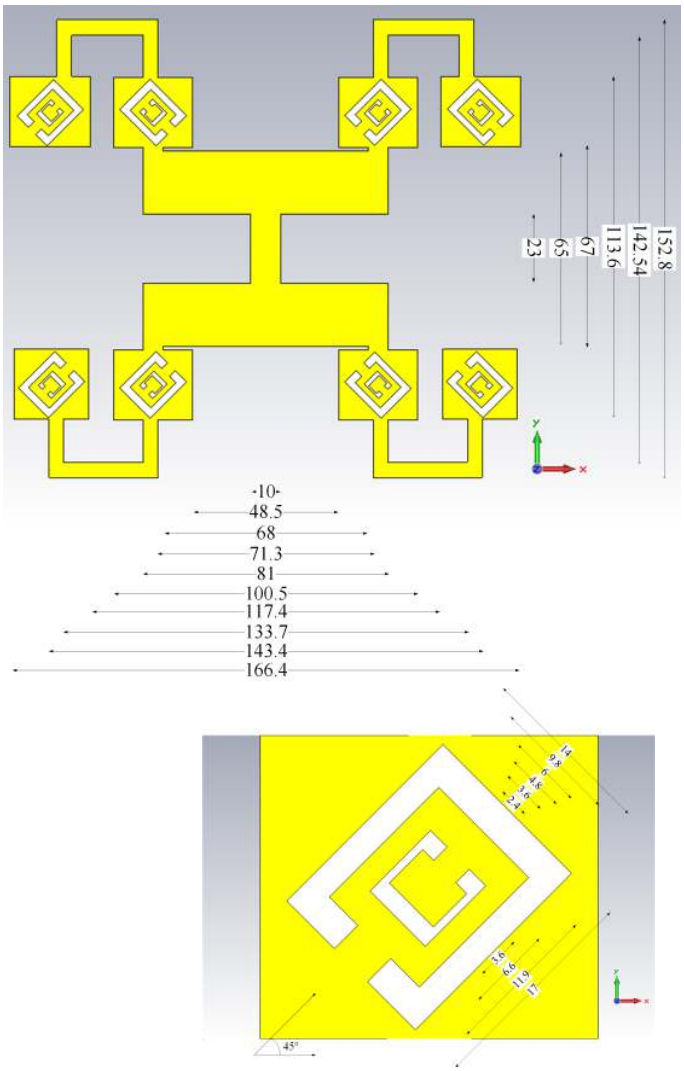

Figure 5.11: (a) Schematic diagram of Rotated-Stepped-Impedance array loaded with CSRRs (b) Schematic diagram of loaded CSRR.

both the required bands, and left shifting the lower band to radiate in the exact 2.4 GHz band.

5.2.3 Results and Discussions

Figure 5.12(a) depicts the Scattering parameter S_{11}, this reflections coefficient shows that very less power is reflected back from 2.423 GHz to 2.5283 GHz, with the minimum going to -19.11 dB at 2.472 GHz, giving a potential bandwidth of 105.3 MHz for the first band of WLAN i.e. 2.4 GHz band. For the second band of WLAN, this antenna

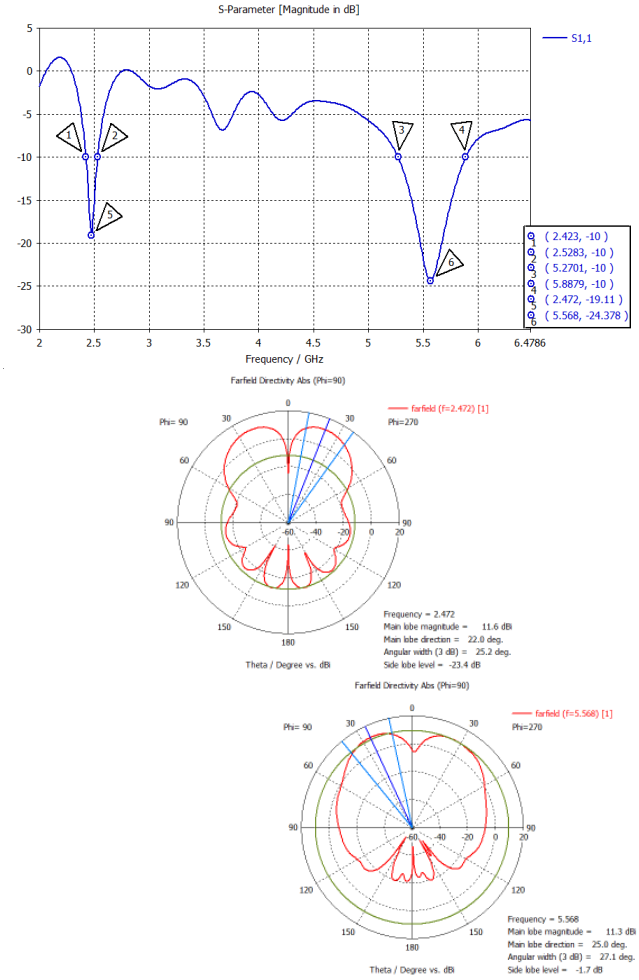

Figure 5.12: (a) Reflection Coefficient. (b) Farfield at first frequency band-2.4 GHz. (c) Farfield at second frequency band-5 GHz

again shows very low return loss from 5.2701 GHz to 5.8879 GHz, likewise the minimum going to -24.378 dB at 5.568 GHz, giving a potential bandwidth of 617.8 MHz for 5 GHz band. Using equation 5.5 [62], most of the power feed to antenna, in these two bands will be utilized by the antenna, and a very less power will be reflected back, giving out very low Standing Wave Ratio of 1.02485 and 1.007325 at 2.472 GHz and 5.568 GHz respectively.

$$SWR = \frac{1 + |\Gamma|}{1 - |\Gamma|} \tag{5.5}$$

where SWR is Standing Wave Ratio for the wave with the reflection coefficient Γ.

Figure 5.12 (b) and (c) shows the absolute farfield directivity, at a fixed azimuthal angle

of 90° in both the bands at 2.472 GHz as well as 5.568 GHz. The antenna has a good directivity because of array type structure, the first band shows a directivity of 11.6 dBi at polar angle of 22° with a 3 dB angular width of 25.2°. The second band shows a directivity of 11.3 dBi at polar angle of 25° with a 3 dB angular width of 27.1°. Since, the design is symmetrical across y-axis, this gives a symmetrical radiation pattern in H-plane, in both the bands. Usage of Complementary Split Ring Resonators in array structure, has improved mainly four result aspects of the design, one is further reduction of return loss in first WLAN band 2.4 GHz, likewise second is also further reduction of return loss in second WLAN band 5 GHz, third is removal of unwanted radiation at 3.845 GHz giving forth a better radiation efficiency in both the radiating bands of WLAN, fourth is left shifting the 2.4 GHz band to radiate suitably in proper band. As the antenna is also covering the band for Bluetooth 2.4 GHz to 2.5 GHz, this configuration can be used for Bluetooth applications as well.

5.3 MPA with Meander Line, U-slot and a slot derived from CSRR

Figure 3.3 shows the basic cavity model [63] which has been extensively used to study microstrip resonators, which says that the rectangular microstrip antenna having metallic patch on the top and metallic ground on the bottom, encloses a rectangular cavity in between which is loaded by a dielectric material. For different sizes of this rectangular patch, different resonant mode configurations are excited in this cavity, whose resonant frequencies [64] are given by

$$\left(f_r\right)_{mnp} = \frac{1}{2\pi\sqrt{\mu\epsilon}}\sqrt{\left(\frac{m\pi}{h}\right)^2 + \left(\frac{n\pi}{L}\right)^2 + \left(\frac{p\pi}{W}\right)^2} \tag{5.6}$$

where W, L, h are the dimensions of antenna, and p, n, m are modes along x, y, z co-ordinates, and μ, ϵ are permeability and permittivity of delectric material present in the cavity. According to this theory, this cavity is bounded along the lateral edges by a

magnetic walls, and from the top and bottom by the electric walls, obviously following the assumptions made in this theory. This cavity model is used in power-return plane [65] structure characterization.

When a traveling Electro-Magnetic Wave (EMW) is intercepted by a perfect conductor, the incident and the reflected wave [66] are of equal amplitude, that is all the incident energy is reflected back by a perfect conductor (with a skin depth=0). Moving towards our design, we have used meander line structure in our patch. Now, considering the fact that the ground here is an approximately perfect conductor (copper), it will reflect all the waves incident on it, towards the patch lying above it, which is mainly a meander line structure. Now, the motivation is, for the part of wave, incident on meander line, which was reflected by the perfect conducting ground below it, is similar to some extent to the scenario of a wave falling on a meander line polarizer (where the unit structure is same, leaving the repetition of same unit and stacking of same layers, only difference comes in analyzing meander line properties in the context of polarization.). Since, a good research is already available for meander line polarizers, this came out to be helpful for analysis of our meander line structure. As shown in Figure 5.13, the MPA is loaded with a meander line, which is known for its good manipulation to current path, this MPA is joined to a microstrip feed through a U-slot antenna. The bottom ground plane of the MPA is also slotted in the pattern of rotated outer ring of a CSRR. Thickness of strips or slots are 1 mm, except for the feeding strip. FR-4 substrate is used with a height of 1.6mm, and thickness of patch metal is .034 mm. The design shows, as shown in Figure 5.14 two bands of radiation, one at 2.33 GHz with a return loss of -29.12 dB, with a bandwidth of 110 MHz, ranging from 2.29 GHz to 2.4 GHz. The second band is at 5.5 GHz, with the return loss going till -24.27 dB and a bandwidth of 220 MHz, ranging from 5.4 GHz to 5.62 GHz. This design with some variations, can be use for WLAN application, as both the band are near to the bands of WLAN bands. Farfield radiation in Figure 5.15 shows a kind of isolation for direction for both the bands, which can be used for some applications. As shown in Figure 5.17, practical result for reflection coefficient, obtained from Vector Network Analyser (VNA) are in matching with the

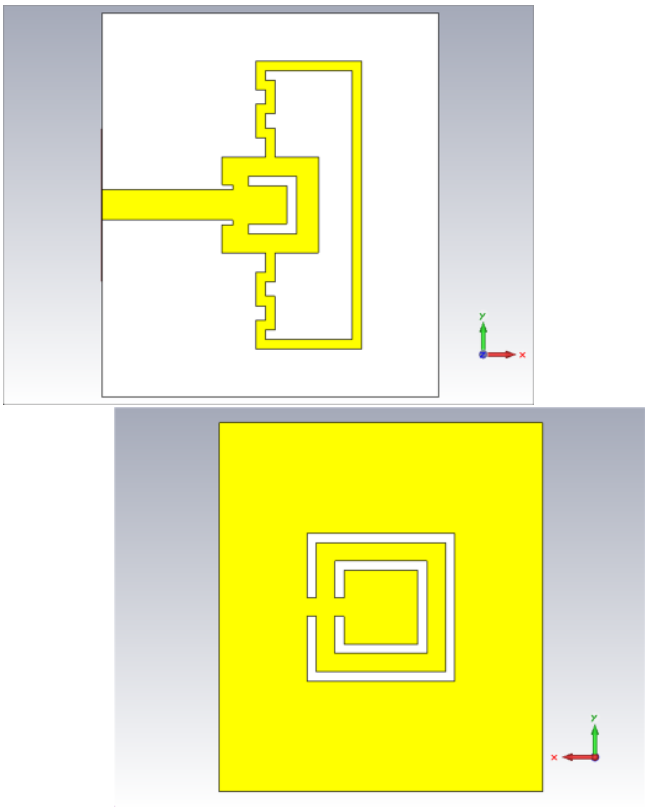

Figure 5.13: (a) Simulated design front (b) Simulated design back.

simulated results, with the lower band shifted to right to 2.925 GHz and S_{11} going to -18.039 dB. The second band is shown at 5.42 GHz with the S_{11} going to -17.2279 dB. Both the bands are showing low return loss, thus validating the design and its simulation results.

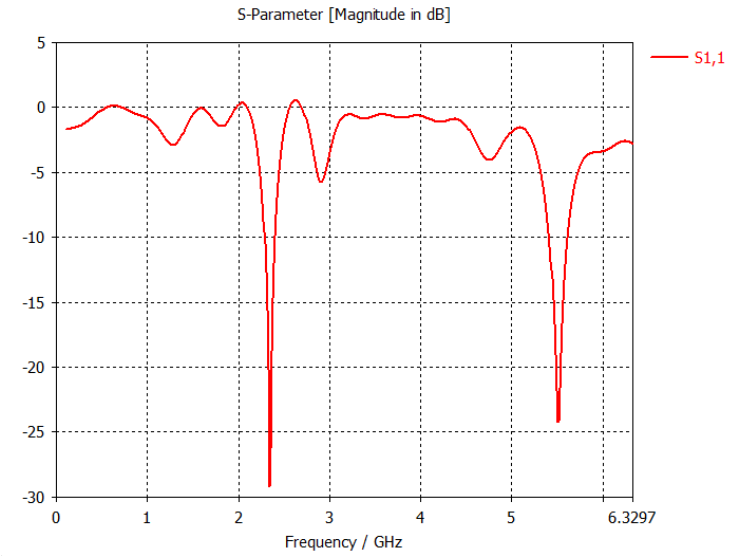

Figure 5.14: Simulated $|S_{11}|$ dB.

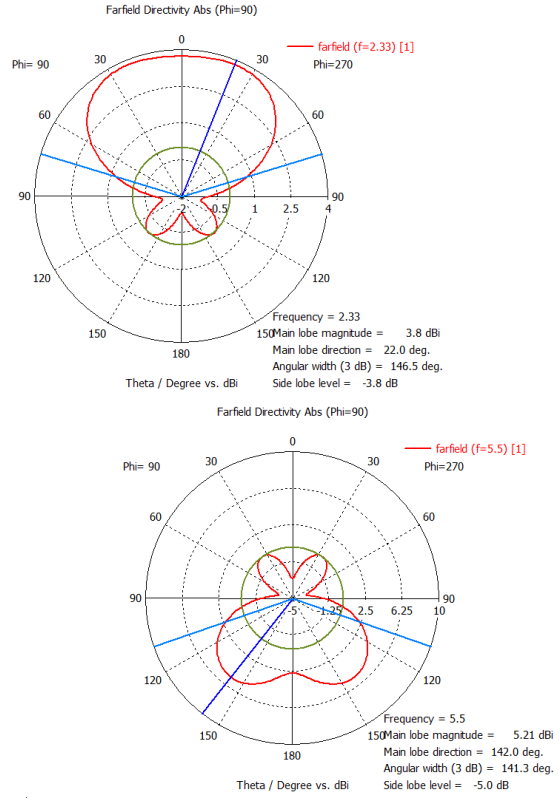

Figure 5.15: (a) Simulated farfield at lower band (b) Simulated farfield at higher band.

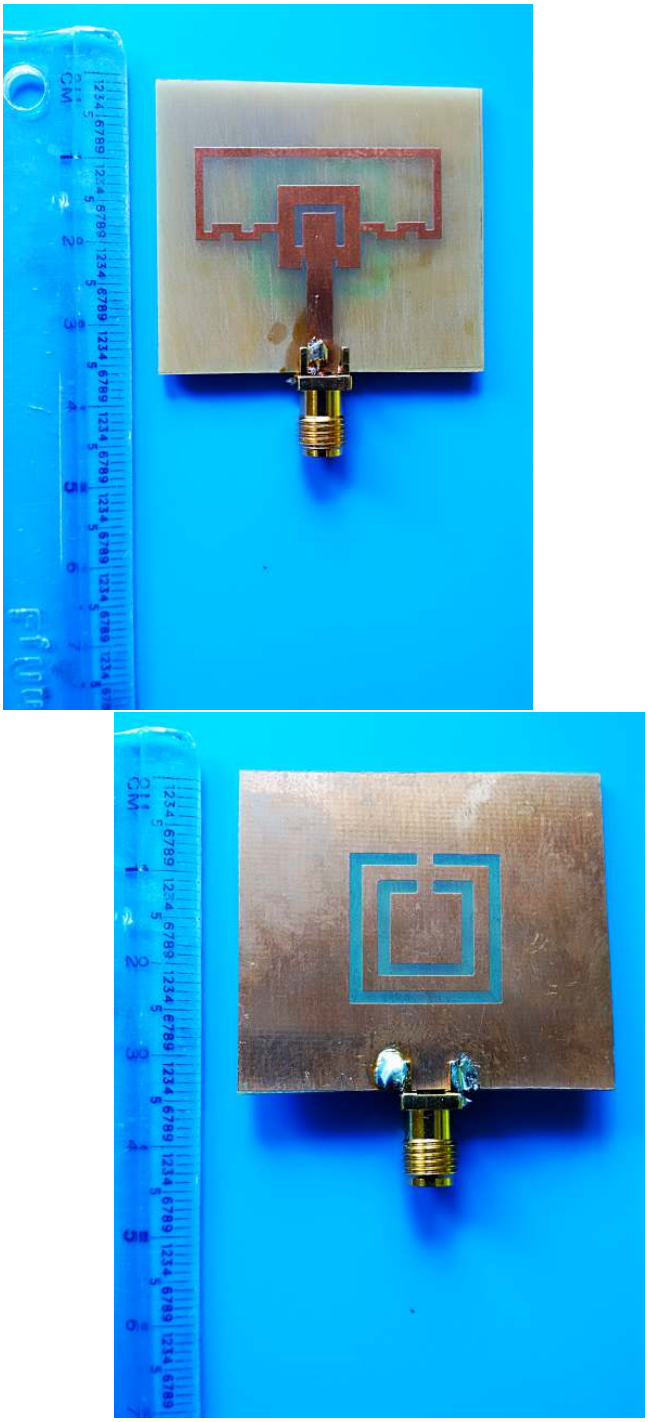

Figure 5.16: (a) Fabricated design front (b) Fabricated design back.

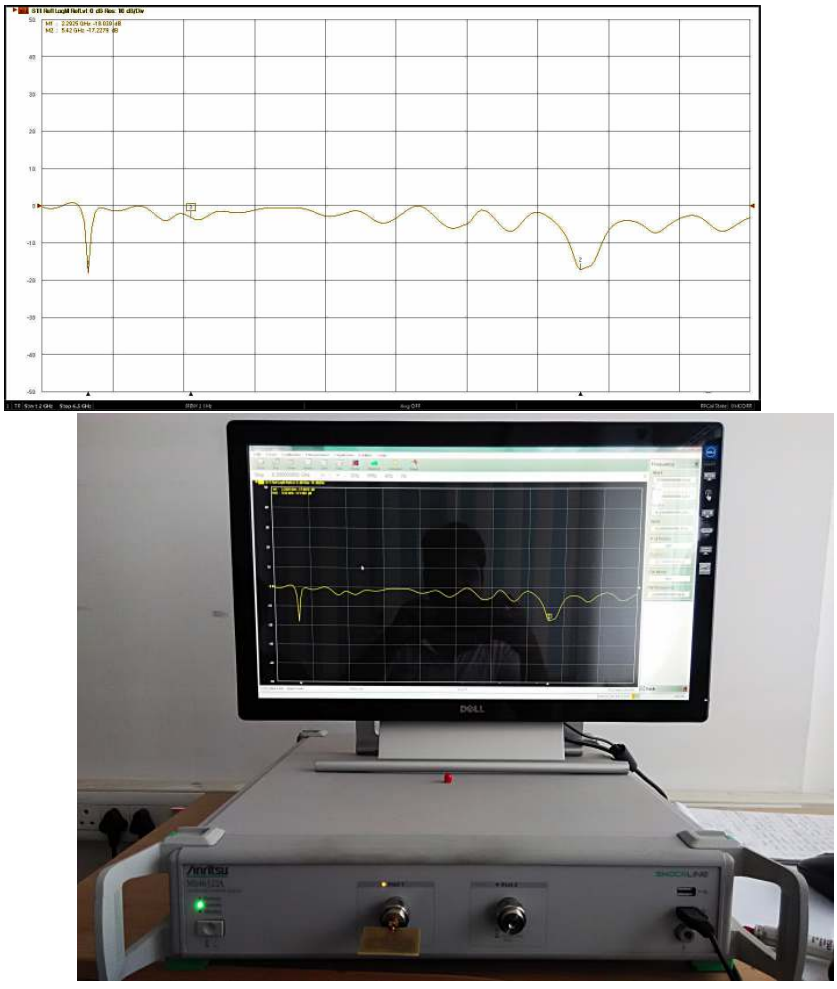

Figure 5.17: (a) VNA results (b) VNA setup while testing.

Chapter 6

Conclusions

CSRRs mainly act as resonators instead of radiators, but the variation in their configuration can add lots of versatility to the MPA, on which they are loaded. CSRRs can be modeled as the resonant L-C circuit, with resistance accounting for losses involved. Single band, double band, and triple band have been obtained from the same design, just with the change in configuration of the CSRRs. Frequency shifting, size miniaturization, and resonance band generation have been done using CSRRs to design some antennas for WLAN application. Microwave stepped-impedance LP filter has been used to remove interferences from higher bands, whereas, array has been proved to enhance the directivity of the overall antenna. Use of meander lines have also been proved to enhance radiations as they provide maneuverability to current paths, but incur greater ohmic losses also. New designs with lower return losses and higher directivity have been modeled, fabricated, and tested.

References

[1] G. A. Deschamps, "Microstrip microwave antennas," in *3rd USAF Symp.on Antennas*, 1953.

[2] H. Gutton and G. Baissinot, "Flat aerial for ultra high frequencies," French Patent No. 703 113, 1955.

[3] E. V. Byron, "A new flush-mounted antenna element for phased array application," in *Proc. Phased-Array Antenna Symp.*, 1970, pp. 187–192.

[4] R. E. Munson, "Single slot cavity antennas assembly," U.S. Patent 3 713 162, Jan. 23, 1973.

[5] Y. T. Lo, D. D. Harrison, D. Solomon, G. A. Deschamps, and F. R. Ore, "Study of microstrip antennas, microstrip phased arrays, and microstrip feed networks," *Rome Air Development Center*, no. TR-77-406, Oct 1977.

[6] J. Nakamura, S. Wakui, and A. Natori, "First-principles evaluations of dielectric constants," in *Nano CMOS, 2006 International Workshop on*, Jan 2006, pp. 236–249.

[7] I. Bady, "Measurement of the complex dielectric constant of very-high-dielectric-constant materials at microwave frequencies," *American Institute of Electrical Engineers, Part I: Communication and Electronics, Transactions of the*, vol. 76, no. 2, pp. 225–228, May 1957.

[8] K. O'Connor and R. Curry, "High voltage characterization of high dielectric constant composites," in *Power Modulator and High Voltage Conference (IPMHVC), 2010 IEEE International*, May 2010, pp. 159–162.

[9] D. Senic, Z. Zivkovic, M. Simic, and A. Sarolic, "Rectangular patch antenna: Design, wideband properties and loss tangent influence," in *Software, Telecommunications and Computer Networks (SoftCOM), 2014 22nd International Conference on*, Sept 2014, pp. 19–23.

[10] P. Pasunoori and A. Engin, "Automated dielectric constant and loss tangent characterization using cavity resonators," in *Electromagnetic Compatibility (EMC), 2011 IEEE International Symposium on*, Aug 2011, pp. 509–513.

[11] M. Zinieris and R. Sloan, "Higher-order modes in dielectric resonators for measurement of loss tangent," *Science, Measurement and Technology, IEEE Proceedings*, vol. 147, no. 2, pp. 91–94, Mar 2000.

[12] B. Mekimah, A. Messai, S. Aris, M. Meriche, and T. Fortaki, "The effect of the loss tangent on the bandwidth of the microstrip antennas in stacked configuration," in *Microwave Symposium (MMS), 2014 14th Mediterranean*, Dec 2014, pp. 1–5.

[13] C.-H. Chou, P.-N. Li, and S.-M. Wu, "The more accurate method to extract dielectric constant and loss tangent of insulated material on microwave frequencies," in *Electronic Packaging Technology Conference, 2005. EPTC 2005. Proceedings of 7th*, vol. 2, Dec 2005, pp. 4 pp.–.

[14] J. Huang, "Microstrip antennas: Analysis, design and applications," in *Modern Antenna Handbook*. John Wiley and Sons,Inc., 2008, ch. 4.

[15] A. Goldsmith, "Overview of wireless communications," in *Wireless Communications*. Cambridge University Press, 2005, ch. 1, pp. 1–26.

[16] (2015) The CST Microwave Studio website. [Online]. Available: https://www.cst.com/Products/CSTMWS

[17] S. U. P. Athanasios Papoulis, "Probaibility, random variables, and stochastic processes," in *Microstrip Patch Antennas*. Tata McGraw Hill, 2011, ch. 5, pp. 123–168.

[18] J. Baena, J. Bonache, F. Martin, R. Sillero, F. Falcone, T. Lopetegi, M. Laso, J. Garcia-Garcia, I. Gil, M. Portillo, and M. Sorolla, "Equivalent-circuit models for split-ring resonators and complementary split-ring resonators coupled to planar transmission lines," *Microwave Theory and Techniques, IEEE Transactions on*, vol. 53, no. 4, pp. 1451–1461, April 2005.

[19] V. Veselago, "The electrodynamics of substances with simultaneously negative values of epsilon and mu," *Soviet Physics Uspekhi*, vol. 10, no. 4, pp. 517–526, February 1968.

[20] R. K. Carver and J. Mink, "Microstrip antenna technology," *Antennas and Propagation, IEEE Transactions on*, vol. 29, no. 1, pp. 2–24, Jan 1981.

[21] H. Attia, L. Yousefi, M. Bait-Suwailam, M. S. Boybay, and O. M. Ramahi, "Enhanced-gain microstrip antenna using engineered magnetic superstrates," *Antennas and Wireless Propagation Letters, IEEE*, vol. 8, pp. 1198–1201, 2009.

[22] R. Jedlicka, M. Poe, and K. Carver, "Measured mutual coupling between microstrip antennas," *Antennas and Propagation, IEEE Transactions on*, vol. 29, no. 1, pp. 147–149, Jan 1981.

[23] M. Bait-Suwailam, O. Siddiqui, and O. M. Ramahi, "Mutual coupling reduction between microstrip patch antennas using slotted-complementary split-ring resonators," *Antennas and Wireless Propagation Letters, IEEE*, vol. 9, pp. 876–878, 2010.

[24] A. Abdel-Rahman, A. Verma, A. Boutejdar, and A. Omar, "Control of bandstop response of hi-lo microstrip low-pass filter using slot in ground plane," *Microwave Theory and Techniques, IEEE Transactions on*, vol. 52, no. 3, pp. 1008–1013, March 2004.

[25] Y. Dong, H. Toyao, and T. Itoh, "Design and characterization of miniaturized patch antennas loaded with complementary split-ring resonators," *Antennas and Propagation, IEEE Transactions on*, vol. 60, no. 2, pp. 772–785, Feb 2012.

[26] W. K. Toh, X. Qing, and Z. N. Chen, "A planar dualband antenna array," *Antennas and Propagation, IEEE Transactions on*, vol. 59, no. 3, pp. 833–838, March 2011.

[27] L. Young, L. Robinson, and C. Hacking, "Meander-line polarizer," *Antennas and Propagation, IEEE Transactions on*, vol. 21, no. 3, pp. 376–378, May 1973.

[28] F. Paredes, G. Gonzalez, J. Bonache, and F. Martin, "Dual-band impedance-matching networks based on split-ring resonators for applications in rf identification (rfid)," *Microwave Theory and Techniques, IEEE Transactions on*, vol. 58, no. 5, pp. 1159–1166, May 2010.

[29] J. Ha, K. Kwon, Y. Lee, and J. Choi, "Hybrid mode wideband patch antenna loaded with a planar metamaterial unit cell," *Antennas and Propagation, IEEE Transactions on*, vol. 60, no. 2, pp. 1143–1147, Feb 2012.

[30] W. Cao, Y. Xiang, B. Zhang, A. Liu, T. Yu, and D. Guo, "A low-cost compact patch antenna with beam steering based on csrr-loaded ground," *Antennas and Wireless Propagation Letters, IEEE*, vol. 10, pp. 1520–1523, 2011.

[31] S. Mishra, R. Gupta, and J. Mukherjee, "Effect of substrate material on radiation characteristics of an uwb antenna," in *Antennas and Propagation Conference (LAPC), 2010 Loughborough*, Nov 2010, pp. 157–160.

[32] C.-H. Chang and K.-L. Wong, "Printed lambda /8 -pifa for penta-band wwan operation in the mobile phone," *Antennas and Propagation, IEEE Transactions on*, vol. 57, no. 5, pp. 1373–1381, May 2009.

[33] R. Munson, "Conformal microstrip antennas and microstrip phased arrays," *Antennas and Propagation, IEEE Transactions on*, vol. 22, no. 1, pp. 74–78, Jan 1974.

[34] R. F. Harrington, *Time-Harmonic Electromagnetic Waves*. New York: McGraw-Hill, 1961.

[35] A. G. Derneryd, "A theoretical investigation of the rectangular microstrip antenna element," *Antennas and Propagation, IEEE Transactions on*, vol. 26, no. 4, pp. 532–535, Jul 1978.

[36] G. Kompa and R. Mehran, "Planar waveguide model for calculating microstrip components," *Electronics Letters*, vol. 11, no. 19, pp. 459–460, September 1975.

[37] E. Hammerstad and O. Jensen, "Accurate models for microstrip computer-aided design," in *Microwave symposium Digest, 1980 IEEE MTT-S International*, May 1980, pp. 407–409.

[38] A. G. Derneryd, "Linearly polarized microstrip antennas," *Antennas and Propagation, IEEE Transactions on*, vol. 24, no. 6, pp. 846–851, Nov 1976.

[39] K. Mousskhani and A. Mirkamali, "A modified broadband transmission line model for rectangular patch antennas," in *Recent Advances in Microwave Theory and Applications, 2008. MICROWAVE 2008. International Conference on*, Nov 2008, pp. 369–371.

[40] Y. Lo, D. Solomon, and W. Richards, "Theory and experiment on microstrip antennas," *Antennas and Propagation, IEEE Transactions on*, vol. 27, no. 2, pp. 137–145, Mar 1979.

[41] W. H. Hayt and J. A. Buck, "Plane wave reflection and dispersion," in *Engineering Electromagnetics*. Tata McGraw Hill Education Private Limited, 2012, ch. 13, pp. 434–476.

[42] M. Xu, H. Wang, and T. Hubing, "Application of the cavity model to lossy power-return plane structures in printed circuit boards," *Advanced Packaging, IEEE Transactions on*, vol. 26, no. 1, pp. 73–80, Feb 2003.

[43] M. Ismail and M. Esa, "Resonant modes configurations for rectangular antenna based on cavity model," in *Communications, 2003. APCC 2003. The 9th Asia-Pacific Conference on*, vol. 3, Sept 2003, pp. 954–958 Vol.3.

[44] Y. Suzuki and T. Chiba, "Computer analysis method for arbitrarily shaped microstrip antenna with multiterminals," *Antennas and Propagation, IEEE Transactions on*, vol. 32, no. 6, pp. 585–590, Jun 1984.

[45] J. Kong, "Analysis of a circular microstrip disk antenna with a thick dielectric substrate," *Antennas and Propagation, IEEE Transactions on*, vol. 29, no. 1, pp. 68–76, Jan 1981.

[46] D. M. Pozar, "Input impedance and mutual coupling of rectangular microstrip antennas," *Antennas and Propagation, IEEE Transactions on*, vol. 30, no. 6, pp. 1191–1196, Nov 1982.

[47] Z. Fan and K.-F. Lee, "Input impedance of rectangular microstrip antennas with a dielectric cover," *Microwave and Optical Technology Letters*, vol. 5, no. 3, pp. 123–125, 1992.

[48] K. Yee, "Numerical solution of initial boundary value problems involving maxwell's equations in isotropic media," *Antennas and Propagation, IEEE Transactions on*, vol. 14, no. 3, pp. 302–307, May 1966.

[49] R. M. Foster, "Directive diagrams of antenna arrays," *Bell System Technical Journal, The*, vol. 5, no. 2, pp. 292–307, April 1926.

[50] C. A. Balanis, "Arrays:linear, planar, circular," in *Antenna Theory*. John Wiley and Sons, 2012, ch. 6, pp. 283–371.

[51] K. M. L. Kai Fong Lee, "Microstrip antenna array," in *Microstrip Patch Antennas*. Imperial College Press, 2011, ch. 17, pp. 487–515.

[52] J. Huang, "A parallel-series-fed microstrip array with high efficiency and low cross-polarization," *Dual-polarized microstrip array with high isolation and low cross-polarization*, pp. 99–103, February 1991.

[53] T. Weiland, "Finite integration method and discrete electromagnetism," in *Computational Electromagnetics*, P. M. C. Carstensen, Ed. Springer Berlin Heidelberg, 2003, ch. 3, pp. 183–198.

[54] W. H. Hayt and J. A. Buck, "Time-varying fields and maxwell's equations," in *Engineering Electromagnetics*. Tata McGraw Hill Education Private Limited, 2012, ch. 10, pp. 306–321.

[55] Y. Dong, H. Toyao, and T. Itoh, "Design and characterization of miniaturized patch antennas loaded with complementary split-ring resonators," *Antennas and Propagation, IEEE Transactions on*, vol. 60, no. 2, pp. 772–785, Feb 2012.

[56] F. Yang and Y. Rahmat-Samii, "Reflection phase characterizations of the ebg ground plane for low profile wire antenna applications," *Antennas and Propagation, IEEE Transactions on*, vol. 51, no. 10, pp. 2691–2703, Oct 2003.

[57] K. M. L. Kai Fong Lee, "Microstrip antenna array," in *Microstrip Patch Antennas*. Imperial College Press, 2011, ch. 17, pp. 487–515.

[58] E. M. T. J. George L. Matthaei, Leo Young, "Low-pass prototype filters obtained by network synthesis methods," in *Microwave Filters, Impedance-Matching Networks, and Coupling Structures*. Artech House, Inc., 1980, ch. 4, pp. 83–162.

[59] D. M. Pozar, "Microwave filters," in *Microwave Engineering*. John Wiley and Sons, Inc., 2012, ch. 8, pp. 380–443.

[60] F. Falcone, T. Lopetegi, J. Baena, R. Marques, F. Martin, and M. Sorolla, "Effective negative- epsiv; stopband microstrip lines based on complementary split ring resonators," *Microwave and Wireless Components Letters, IEEE*, vol. 14, no. 6, pp. 280–282, June 2004.

[61] J. Baena, J. Bonache, F. Martin, R. Sillero, F. Falcone, T. Lopetegi, M. Laso, J. Garcia-Garcia, I. Gil, M. Portillo, and M. Sorolla, "Equivalent-circuit models for split-ring resonators and complementary split-ring resonators coupled to planar transmission lines," *Microwave Theory and Techniques, IEEE Transactions on*, vol. 53, no. 4, pp. 1451–1461, April 2005.

[62] (2015) The Wikipedia website. [Online]. Available: https://en.wikipedia.org/wiki/SWR

[63] Y. Lo, D. Solomon, and W. Richards, "Theory and experiment on microstrip antennas," *Antennas and Propagation, IEEE Transactions on*, vol. 27, no. 2, pp. 137–145, Mar 1979.

[64] M. Ismail and M. Esa, "Resonant modes configurations for rectangular antenna based on cavity model," in *Communications, 2003. APCC 2003. The 9th Asia-Pacific Conference on*, vol. 3, Sept 2003, pp. 954–958 Vol.3.

[65] M. Xu, H. Wang, and T. Hubing, "Application of the cavity model to lossy power-return plane structures in printed circuit boards," *Advanced Packaging, IEEE Transactions on*, vol. 26, no. 1, pp. 73–80, Feb 2003.

[66] W. H. Hayt and J. A. Buck, "Plane wave reflection and dispersion," in *Engineering Electromagnetics*. Tata McGraw Hill Education Private Limited, 2012, ch. 13, pp. 434–476.

List of Publications

1. "Dual Band High Directivity Microstrip Patch Antenna Rotated-Stepped-Impedance Array Loaded with CSRRs for WLAN Applications" communicated to "International Journal of Microwave Science and Technology", Hindawi Publishing Corporation vide receipt no. 494235.

2. MPA with meander line, U-slot and modification of CSRR for WLAN applications, to be communicated.